CALCULATION OF EFFECTIVE ELECTROMAGNETIC PARAMETERS OF HELIX LOADED COMPOSITES

by

Christina Manolatou

Submitted to the Department of Electrical Engineering and
Computer Science
in partial fulfillment of the requirements for the degree of

MASTER OF SCIENCE IN ELECTRICAL ENGINEERING AND
COMPUTER SCIENCE

at the

MASSACHUSETTS INSTITUTE OF TECHNOLOGY

May 1995

Author . . . .
Department of Electrical Engineering and Computer Science
May 12, 1995

Certified by . . . .
Jin Au Kong
Professor of Electrical Engineering
Thesis Supervisor

Certified by . . . .
R. T. Shin
Assistant Group Leader, MIT Lincoln Laboratory
Thesis Supervisor

Accepted by . . . .
Frederic R. Morgenthaler
Chairman, Departmental Committee on Graduate Students

CALCULATION OF EFFECTIVE ELECTROMAGNETIC PARAMETERS OF HELIX LOADED COMPOSITES

by

Christina Manolatou

Abstract

There is currently a great interest in studying the electromagnetic response of helix loaded composites. There have been many works in the literature that model such materials as artificial chiral media. The objective is to understand the dependence of the electromagnetic response of the artificial medium on the inclusion and the host medium parameters. Therefore, a theoretical model is needed to express this dependence and to be used in the design of composites with desirable absorption and polarization characteristics.

In this work, a theoretical model is proposed for characterizing the response of artificial media made up of randomly oriented helices in a host medium, based on a description of these materials with the constitutive relations of effective chiral media. The macroscopic electromagnetic parameters are calculated in terms of helix and host medium parameters.

The approach taken is to first solve the scattering by a single helix numerically using the method of moments (MoM) under a thin wire approximation in order to calculate the helix polarizabilities. The effective electromegnetic parameters of the composite medium are then obtained by applying an extension of the standard Maxwell-Garnett mixing formula to include chirality. Using the effective electromagnetic parameeters that are calculated by this approach, reflection and transmission calculations are performed.

It is found that the variation of the electromagnetic response with frequency is well predicted by the theoretical model and the expected resonance frequencies are obtained due the accuracy of the method of moments. However, the comparison with published measurement results reveals the limitations of the model to low inclusions and low frequencies.

Due to these limitations an alternate approach is investigated for periodic structures consisting of infinite two-dimensional arrays of aligned helices. This approach

is based on an exact MoM solution of the integral equation for the induced currents, using a periodic Green's function. The formulation derived can be used to find the scattered fields. The reflection and transmission coefficients for a given incidence could then be inverted to give the effective EM parameters.

Thesis Supervisor: Jin Au Kong
Title: Professor of Electrical Engineering

Thesis Supervisor: R. T. Shin
Title: Assistant Group Leader, MIT Lincoln Laboratory

ACKNOWLEDGMENTS

To My Family

Contents

List of Figures

11

Chapter 1

Introduction

1.1 Optical Activity - Chirality

Optical activity has been known since the 19th century. Pasteur, or isotropic chiral, materials have long been distinguished by their ability to rotate the plane of polarization of light passing through them. Arago (1811) and Biot (1812) discovered the first effects of optical activity in anisotropic gypsum and quartz crystals. These discoveries led to the problem of determining the cause of optical activity. In 1848 Pasteur solved the problem by postulating that the optical activity in a medium is caused by the chirality of its molecules [14]. Chiral materials display handedness (from where the term chiral which means handed, comes) in their microstructure which denotes a lack of space inversion symmetry. That is, they exist in two distinct forms, mirror images of each other, that cannot be superimposed (stereoisomeres or enantiomeres).

Chirality is a purely geometric notion which refers to the lack of symmetry of an object. By definition, an object is chiral if it cannot be brought into congruence with its mirror image by translation or rotation. Most of the work on chiral media has been done by physical chemists who have developed polarimetric techniques to investigate molecular and crystall structures. But chirality is a phenomenon which can be found in everyday life. Helices, Möbius strips, and, of course our hands are examples of chiral objects found everywhere (Figure 1-1). The rotation of polarization of linearly polarized light passing through a substance whose molecules possess a

13
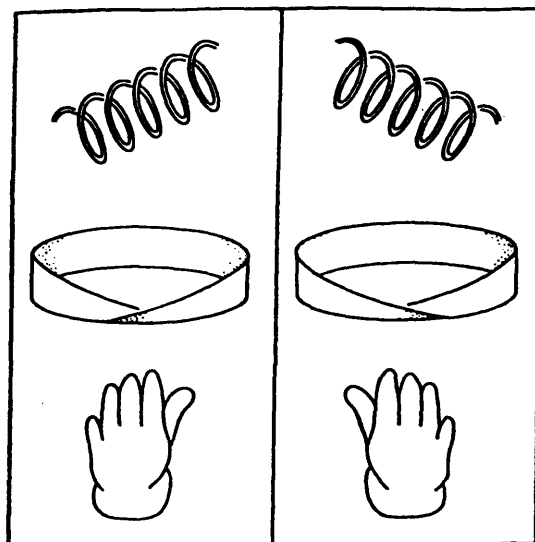
Figure 1-1: Handed objects and their mirror images

certain handedness, such as sugar, is the most familliar of the various chiral effects
that occur in nature. Optical rotation and circular dichroism for example is exhibited
by certain molecules, such as L- and D-type stereoisomers. As the name suggests, such
phenomena are noticeable at optical wavelengths (400 - 700 nm). Due to the right- or
left- handed configuration of their molecules, such media can distinguish between right
and left circularly polarized waves in the visible range. When an electromagnetic wave
travels through a medium consisting of chiral molecules it is forced to adapt to the
handedness of the molecules. In such media, the linearly polarized light decomposes
into two circularly polarized waves.

The rotation of the polarization plane is the manifestation of circular birefringence,
which is the difference in the refractive indices for left and right circularly polarized
electromagnetic waves. Chiral effects which have proved useful in molecular structure
determinations are circular dichroism (the differential absorption of right and left
circularly polarized light if the medium is lossy), optical rotatory dispersion (the
dependence on the frequency of the angle of rotation of the plane of polarization) and
circular intensity difference (the difference in scattered intensity between right and
left circularly polarized light incident on the medium) [16]. Also, the Cotton effect,
is rapid variations of the angle of rotation and the attenuation with frequency.

14

The effects of optical activity are observed when the wavelength is small enough to discriminate the handedness of the chiral particles. Thus, substances which are optically active in light wave frequencies are inactive in microwave and millimeter wave frequencies. However, the analog at lower frequencies can be artificially constructed.

Drude was the first to suggest constitutive relations for optically active media. The measure of optical activity in these relations can be called chirality parameter and contains information also for the circular dichroism.

1.2   Wave Propagation in Chiral Media

Because a chiral medium responds differently to an electromagnetic excitation, depending upon the handedness with which it is endowed, its contitutive relations are not the usual ones. The constitutive relations $\overline{D} = \epsilon\overline{E}$ and $\overline{B} = \mu\overline{H}$ are not compatible with the phenomena of birefringence and dichroism. Within the framework of classical electromagnetics, the optical rotary dispersion and circular dichroism properties of chiral materials can be explained by a magnetoelectric coupling effect [9]. That is, the effective polarization density $\overline{P}_e$ (effective magnetization density $\overline{P}_m$) is induced not only by the electric (magnetic) field but also on the magnetic (electric) field. Thus, a chiral medium is described by constitutive relations in which the electric and the magnetic fields are coupled. That is the electric and the magnetic flux density are induced by both the electric and the magnetic fields. Several forms exist in the literature for the constitutive relations for isotropic chiral media. A notation commonly used in the literature (Drude-Born-Fedorov relations [9]) is:

$$\overline{D} = \epsilon\overline{E} + \epsilon\beta\nabla \times \overline{E} \qquad (1.1)$$

$$\overline{B} = \mu\overline{H} + \mu\beta\nabla \times \overline{H} \qquad (1.2)$$

These relations reflect the isotropic but non-centrosymmetric nature of the materials via the terms $\nabla \times \overline{E}$ and $\nabla \times \overline{H}$ [24]. The scalar material constants ϵ and μ are the dielectric permittivity and the magnetic permeability of the medium, respectively.

15

The scalar constant β (with units of length) is the chirality parameter and has a positive real part if the medium is right handed and a negative real part for left handed medium. Because chiral media are reciprocal bi-isotropic media the coupling between the electric and the magnetic field is described by the same parameter. Thus a chiral material is characterized by three complex, frequency dependent properties. It may be readily observed that because chirality is manifested through the terms $\nabla \times \overline{E}$ and $\nabla \times \overline{H}$, it is absent for static or even quasi-static fields.

In optical frequencies, it is expected that β will be a very small quantity around 10^{-10}m. However the origins of a nonzero β are not necessarily molecular. Electromagnetic waves can recognize the handedness of a chiral objet primarily due to their transverse nature. Thus, at microwave frequencies the chirality parameter can be as big as $\beta \simeq 10^{-3}$m, since it is possible to introduce much higher volume fractions of the chiral microstructure [26].

An alternate but equivalent notation is [9]:

$$\overline{D} = \epsilon'\overline{E} + i\kappa\sqrt{\mu_0\epsilon_0}\,\overline{H} \tag{1.3}$$

$$\overline{B} = \mu'\overline{H} - i\kappa\sqrt{\mu_0\epsilon_0}\,\overline{E} \tag{1.4}$$

where κ is the chirality parameter and is dimensionless.

The relations between notations (1.1), (1.2) and (1.3), (1.4) are:

$$\epsilon' = \frac{\epsilon}{1 - \omega^2\mu\epsilon\beta^2} \tag{1.5}$$

$$\mu' = \frac{\mu}{1 - \omega^2\mu\epsilon\beta^2} \tag{1.6}$$

$$\kappa\sqrt{\mu_0\epsilon_0} = \frac{\omega\mu\epsilon\beta}{1 - \omega^2\mu\epsilon\beta^2} \tag{1.7}$$

and:

$$\epsilon = \epsilon'\left(1 - \frac{\kappa^2}{n^2}\right) \tag{1.8}$$

$$\mu = \mu'\left(1 - \frac{\kappa^2}{n^2}\right) \tag{1.9}$$

16

$$k_0 \beta \;\; = \;\; \frac{\kappa}{n^2 - \kappa^2} \tag{1.10}$$

where $n = \sqrt{\epsilon'\mu'}/\sqrt{\epsilon_0\mu_0}$ and $k_0 = \omega\sqrt{\epsilon_0\mu_0}$.

Using a decomposition first proposed by Bohren [4], it can be shown that left and right circularly polarized fields are the eigenstates of polarization that propagate with a different phase velocity and attenuation. The constitutive relations (1.1), (1.2) in conjunction with Maxwell's equations for source free space:

$$\nabla \times \overline{E} \;\; = \;\; i\omega\overline{B} \tag{1.11}$$

$$\nabla \times \overline{H} \;\; = \;\; -i\omega\overline{D} \tag{1.12}$$

$$\nabla \cdot \overline{B} \;\; = \;\; 0 \tag{1.13}$$

$$\nabla \cdot \overline{D} \;\; = \;\; 0 \tag{1.14}$$

give the equations:

$$\nabla^2 \cdot \begin{bmatrix} \overline{E} \\ \overline{H} \end{bmatrix} = [K]^2 \begin{bmatrix} \overline{E} \\ \overline{H} \end{bmatrix} \tag{1.15}$$

where the matrix K is given by:

$$[K] = \frac{1}{1 - k^2\beta^2} \begin{bmatrix} k^2\beta & i\omega\mu \\ -i\omega\epsilon & k^2\beta \end{bmatrix} \tag{1.16}$$

where $k = \omega\sqrt{\mu\epsilon}$ and a $e^{-i\omega t}$ time dependence is assumed.

The fields in such a medium also satisfy the equations:

$$\nabla \times \begin{bmatrix} \overline{E} \\ \overline{H} \end{bmatrix} \;\; = \;\; [K] \begin{bmatrix} \overline{E} \\ \overline{H} \end{bmatrix} \tag{1.17}$$

$$\nabla \cdot \begin{bmatrix} \overline{E} \\ \overline{H} \end{bmatrix} \;\; = \;\; \begin{bmatrix} 0 \\ 0 \end{bmatrix} \tag{1.18}$$

The characteristic modes of the medium can be found by diagonalizing the above

equation. A linear transformation of the electromagnetic field:

$$\begin{bmatrix} \overline{E} \\ \overline{H} \end{bmatrix} = [A] \begin{bmatrix} \overline{Q}_L \\ \overline{Q}_R \end{bmatrix} \tag{1.19}$$

diagonalizes K:

$$[\Lambda] = [A]^{-1} [\Lambda] [A] \tag{1.20}$$

where

$$[\Lambda] = \begin{bmatrix} k_L & 0 \\ 0 & k_R \end{bmatrix} \tag{1.21}$$

$$[A] = \begin{bmatrix} 1 & a_R \\ a_L & 1 \end{bmatrix} \tag{1.22}$$

where

$$k_R = \frac{k}{1 + k\beta} \tag{1.23}$$

$$k_L = \frac{k}{1 - k\beta} \tag{1.24}$$

and

$$a_R = -i\frac{k_R(1 - \beta^2\omega^2\epsilon\mu) + \beta\omega^2\epsilon\mu}{\omega\epsilon} = -i\eta \tag{1.25}$$

$$a_L = -i\frac{k_L(1 - \beta^2\omega^2\epsilon\mu) - \beta\omega^2\epsilon\mu}{\omega\mu} = -\frac{i}{\eta} \tag{1.26}$$

The waves $\overline{Q}_L$ and $\overline{Q}_R$ are the eigenvectors or the characteristic polarizations of the medium and satisfy the equations:

$$\nabla^2 \cdot \begin{bmatrix} \overline{Q}_L \\ \overline{Q}_R \end{bmatrix} + \begin{bmatrix} k_L^2 & 0 \\ 0 & k_R^2 \end{bmatrix} \begin{bmatrix} \overline{Q}_L \\ \overline{Q}_R \end{bmatrix} = \begin{bmatrix} 0 \\ 0 \end{bmatrix} \tag{1.27}$$

$$\nabla \times \begin{bmatrix} \overline{Q}_L \\ \overline{Q}_R \end{bmatrix} = \begin{bmatrix} k_L & 0 \\ 0 & -k_R \end{bmatrix} \begin{bmatrix} \overline{Q}_L \\ \overline{Q}_R \end{bmatrix} \tag{1.28}$$

$$\nabla \cdot \begin{bmatrix} \overline{Q}_L \\ \overline{Q}_R \end{bmatrix} = \begin{bmatrix} 0 \\ 0 \end{bmatrix} \tag{1.29}$$

In the above relations, $\overline{Q}_L$ represents a left hand circularly polarized wave (LCP) and

$\overline{Q}_R$ a right hand circularly polarized (RCP) wave propagating with wavenumbers k_L and k_R, respectively. Hence the left and right handed CP waves travel with different phase velocities and this gives rise to the rotation in the plane of polarization when linearly polarized light passes through the medium. The LCP waves travel faster than RCP waves inside the left handed medium and vice versa. If, in addition, the medium is lossy, that is k is complex, the two eigenwaves will experience different attenuation resulting in an elliptically polarized wave with a rotation of the major axis of the ellipse (dichroism).

1.3 Artificial Chiral Media

While optical activity occurs in nature in certain materials at optical frequencies, the analog at lower frequencies is artificially constructed. Such materials could be described as artificial chiral media. These media also exhibit, typically in the microwave region, the phenomena of optical activity mentioned above (circular birefringence, rotatory dispersion, and circular dichroism). The discovery of such a phenomenon is attributed to Lindmann (early 1900's) [12],[13] who measured the rotation of the plane of polarization for a collection of wire helices in the wavelength range 12 to 34 cm. It was found that a collection of randomly oriented right-handed helices would rotate the plane of polarization of a linearly polarized wave one way but that a similar collection of left-handed helices would rotate the plane of polarization the opposite way.

Since chirality is related to handedness and handedness is related to optical activity and since electromagnetic waves can discriminate between objects of different handedness owing to their transverse nature, it is not surprising that the interaction between an electromagnetic wave and a collection of randomly oriented chiral objects can be such as to rotate the plane of polarization of the wave to the right or to the left depending on the handedness of the objets. That is, effectively chiral media can be constructed by embedding chiral microstructures in a host medium. The microstructure should be large enough that the electromagnetic wave in the matrix

can appreciate its handedness; at the same time the microstructure size should be small enough that the composite medium, consisting of a chiral phase is effectively homogeneous but chiral [18],[23].

In recent years interest has grown in understanding the properties, at microwave frequencies of chiral composites comprising conducting chiral objects such as helices embedded in a dielectric host medium. Guire et al. (1990) [21] measured the rotatory dispersion for artificial chiral composites, which were made by embedding small helices in a nonchiral host medium. They reported that the rotation angle was proportional to the volume concentration of the helices. Besides the rotatory dispersion, the reflection characteristics from metal backed chiral composites were also reported and it was concluded that a distinct difference in both the rotation and the reflection characteristics can be observed between chiral and nonchiral composites. This work appears to support the theoretical modeling work of Varadan et al. (1987) [22], which predicted that chirality in a material not only affects the polarization characteristics of a propagating wave, but also affects the reflection, transmission, and attenuation characteristics.

By varying concentrations and the sizes of chiral inclusions, the properties of the composite medium may be altered to suit desired polarization characteristics. Chiral composites can also be attractive as highly efficient absorbers. These absorption characteristic are attributed to multiple scattering in conjunction with mode conversion from right to left hand polarized waves [26].

1.4 Description of Thesis

In Chapter 2 the transmission and reflection for chiral media are studied, based on the principles of wave propagation presented in this chapter. The effect of chirality in enhancing the absorption by a low loss dielectric material is examined by calculating the reflection coefficients for a chiral slab over a perfect conductor. The transmission coefficients for a chiral slab in air are also derived and the effects of optical activity (rotation of polarization and dichroism) are related to the effective parameters

through a general measurement technique.

In Chapter 3 the modelling of artificial chiral media is discussed. The standard Maxwell-Garnett mixing formula and its extension to effective chiral media, are presented and the assumptions and limitations inherent in this formula are reviewed.

Chapter 4 presents the modelling work. The problem of electromagnetic scattering by a single helix is solved numerically using a method of moments (Galerkin's method) for the induced currents under a thin wire approximation. Then, the equivalent electric and magnetic dipole moments are calculated and the helix polarizabilities obtained as scalar quantities by averaging over orientation and spin of helix. The Maxwell-Garnett mixing formula is then applied to give the effective EM parameters. Reflection and transmission calculations are also performed and our theoretical predictions are compared to published results. A sensitivity study is also performed and finally the accuracy of the model used is discussed.

Due to the limitations of the Maxwell-Garnett mixing formula to low frequencies and low chiral inclusions, another approach will also be investigated in chapter 5. This is based on a method of moments solution of the exact integral equation for a medium made up of periodically spaced helices. The periodic properties of the medium allow a reduction of the scattering problem to that of a single helix with the use of the periodic Green's function. Our objective in this case is to obtain the effective EM parameters by inversion of reflection and transmission coefficients from a layer of finite thickness.

Chapter 2

Reflection and Transmission Characteristics

2.1 Introduction

The reason that wave propagation and scattering characteristics are so different in chiral media is attributed to mode conversion from LCP to RCP and vice versa. The induced surface current and surface charge densities at the boundary of a chiral material are quite different of those in a non-chiral material [2]. An incident linearly polarized wave will give rise to LCP and RCP inside the inclusion made of chiral material, and these fields propagate with different velocities. Hence if there are several interfaces between chiral and nonchiral materials, we expect enhanced multiple scattering due to mode conversion, and if the host material or inclusion is lossy, this would lead to increase absorption of the wave as it undergoes multiple scattering. Thus, chiral composites can be attractive as highly efficient absorbers. For example, it can be shown theoretically that by endowing low loss dielectric composites with chiral properties the reflected power can be cut down by a factor of 4 or more for the case of a plane coating on a perfectly conducting surface [22].

The field transmitted through a chiral composite layer is elliptically polarized for a normally incident, linearly polarized wave. The major axis of the polarization ellipse is rotated with respect to the polarization of the incident wave. The ellipticity is

positive when the LCP wave is more absorbed than the RCP wave and the transmitted field is right elliptically polarized. Otherwise the transmitted field is left elliptically polarized.

In this chapter the reflection and transmission coefficients for a chiral slab of given thickness are derived and then used to determine the electromagnetic properties of a chiral sample based on transmission and reflection measurements.

2.2   Metal Backed Chiral Slab

Consider first the case of general oblique incidence on a chiral slab which occupies the region $0 \leq z \leq d$. The region $z \leq 0$ is free space while the plane $z = d$ is assumed to be perfectly conducting. This geometry describes a metallic surface coated with a chiral layer of thickness d.

The incidence wave is:

$$\overline{E}^i = \left(A_H \cos \theta_0 \hat{x} + A_E \hat{y} - A_H \sin \theta_0 \hat{z}\right) \exp\left[i k_0 \left(\sin \theta_0 x + \cos \theta_0 z\right)\right] \qquad (2.1)$$

$$\overline{H}^i = \frac{1}{i \omega \mu_0} \nabla \times \overline{E}^i$$

where $A_E \neq 0$, $A_H = 0$ refer to TE polarization while $A_E = 0$, $A_H \neq 0$ refer to TE polarization.

The reflected wave obeys Snell's law of reflection but is composed of two circularly polarized waves. On the other hand, two distinct wavenumbers exist in the chiral medium giving rise also to two circularly polarized waves, (left handed and right handed) which propagate with different phase velocities in the chiral medium. Each, however, still obeys Snell's law of refraction and is therefore inclined differently to the chiral-achiral interface [2]. Consequently, the power reflected by such an interface is quite different from that which can be calculated quite easily by ignoring the handedness.

The reflected wave is:

$$\overline{E^r} = (-R_{TM}A_H \cos\theta_0 \hat{x} + R_{TE}A_E \hat{y} + R_{TM}A_H \sin\theta_0 \hat{z})\exp\left[ik_0\left(\sin\theta_0 x - \cos\theta_0 z\right)\right]$$
(2.2)

$$\overline{H^r} = \frac{1}{i\omega\mu_0}\nabla \times \overline{E^r}$$

where R_{TE} and R_{TM} are the reflection coefficients for TE and TM polarization, respectively.

The eigenwaves propagating in the chiral layer are the sum of a forward and a backward travelling waves:

$$\overline{Q}_{\substack{L\\R}} = \overline{A}_{\substack{L\\R}}\exp\left[ik_{\substack{L\\R}}\left(\sin\theta_{\substack{L\\R}}x + \cos\theta_{\substack{L\\R}}z\right)\right] + \overline{B}_{\substack{L\\R}}\exp\left[ik_{\substack{L\\R}}\left(\sin\theta_{\substack{L\\R}}x - \cos\theta_{\substack{L\\R}}z\right)\right]$$
(2.3)

where $\theta_{\substack{L\\R}}$ denote the angles of inclination for the LCP and RCP waves.

The polarization of $\overline{Q}_{\substack{L\\R}}$ is derived using the equations (1.28):

$$i\overline{k}_{\substack{L\\R}} \times \overline{Q}_{\substack{L\\R}} = \pm k_{\substack{L\\R}}\overline{Q}_{\substack{L\\R}}$$
(2.4)

thus:

$$\begin{aligned}
\overline{Q}_{\substack{L\\R}} &= A_{\substack{L\\R}}\left(\cos\theta_{\substack{L\\R}}\hat{x} \pm i\hat{y} - \sin\theta_{\substack{L\\R}}\hat{z}\right)\exp\left[ik_{\substack{L\\R}}\left(\sin\theta_{\substack{L\\R}}x + \cos\theta_{\substack{L\\R}}z\right)\right] \\
&+ B_{\substack{L\\R}}\left(\cos\theta_{\substack{L\\R}}\hat{x} \mp i\hat{y} - \sin\theta_{\substack{L\\R}}\hat{z}\right)\exp\left[ik_{\substack{L\\R}}\left(\sin\theta_{\substack{L\\R}}x - \cos\theta_{\substack{L\\R}}z\right)\right]
\end{aligned}$$
(2.5)

that represent a superposition of forwards and backwards travelling circularly polarized waves.

The fields in the chiral medium are:

$$\overline{E}_{ch} = \overline{Q}_L + a_R\overline{Q}_R$$
(2.6)

$$\overline{H}_{ch} = a_L\overline{Q}_L + \overline{Q}_R$$
(2.7)

where $a_R = i\eta$, $a_L = i/\eta$ and $\eta = \sqrt{\mu/\epsilon}$.

Next, we apply the boundary conditions at the intefaces and phase matching:

25

at $z = 0$:

$$\hat{x} \cdot \left(\overline{E}^i + \overline{E}^r - \overline{E}^{ch} \right) = 0 \qquad (2.8)$$

$$\hat{x} \cdot \left(\overline{H}^i + \overline{H}^r - \overline{H}^{ch} \right) = 0 \qquad (2.9)$$

$$\hat{y} \cdot \left(\overline{E}^i + \overline{E}^r - \overline{E}^{ch} \right) = 0 \qquad (2.10)$$

$$\hat{y} \cdot \left(\overline{H}^i + \overline{H}^r - \overline{H}^{ch} \right) = 0 \qquad (2.11)$$

at $z = d$:

$$\hat{x} \cdot \overline{E}^{ch} = 0 \qquad (2.12)$$

$$\hat{y} \cdot \overline{E}^{ch} = 0 \qquad (2.13)$$

Phase matching: $k_0 \sin \theta_0 = k_{L \atop R} \sin \theta_{L \atop R}$

Thus we get a 6×6 system of equations which can be solved for the reflection coefficients R_{TE}, R_{TM}:

TE polarization:

$$R_{TE} = -\frac{[\cos(k_L \cos \theta_L d) + \cos(k_R \cos \theta_R d)] + i\frac{\eta}{\eta_0} \cos \theta_0 \left[\frac{\sin(k_L \cos \theta_L d)}{\cos \theta_L} + \frac{\sin(k_R \cos \theta_R d)}{\cos \theta_R} \right]}{[\cos(k_L \cos \theta_L d) + \cos(k_R \cos \theta_R d)] - i\frac{\eta}{\eta_0} \cos \theta_0 \left[\frac{\sin(k_L \cos \theta_L d)}{\cos \theta_L} + \frac{\sin(k_R \cos \theta_R d)}{\cos \theta_R} \right]}$$
$$(2.14)$$

TM polarization:

$$R_{TM} = -\frac{[\cos(k_L \cos \theta_L d) - \cos(k_R \cos \theta_R d)] + i\frac{\eta_0}{\eta} \cos \theta_0 \left[\frac{\sin(k_L \cos \theta_L d)}{\cos \theta_L} - \frac{\sin(k_R \cos \theta_R d)}{\cos \theta_R} \right]}{[\cos(k_L \cos \theta_L d) - \cos(k_R \cos \theta_R d)] - i\frac{\eta_0}{\eta} \cos \theta_0 \left[\frac{\sin(k_L \cos \theta_L d)}{\cos \theta_L} - \frac{\sin(k_R \cos \theta_R d)}{\cos \theta_R} \right]}$$
$$(2.15)$$

In the case of zero chirality $\theta_{L \atop R} = \theta$ and $k_L = k_R = k$, thus:

$$R_{TE} = \frac{1 + i\frac{\eta}{\eta_0} \frac{\cos \theta}{\cos \theta_0} \tan(k \cos \theta d)}{1 - i\frac{\eta}{\eta_0} \frac{\cos \theta}{\cos \theta_0} \tan(k \cos \theta d)} \qquad (2.16)$$

$$R_{TM} = \frac{1 + i\frac{\eta_0}{\eta} \frac{\cos \theta_0}{\cos \theta} \tan(k \cos \theta d)}{1 - i\frac{\eta_0}{\eta} \frac{\cos \theta_0}{\cos \theta} \tan(k \cos \theta d)} \qquad (2.17)$$

26

In the case of normal incidence the above expressions reduce to:

$$R_{TE} = R_{TM} = \frac{1 + i\frac{\eta}{\eta_0}\tan\left(\frac{k_L + k_R}{2}d\right)}{1 - i\frac{\eta}{\eta_0}\tan\left(\frac{k_L + k_R}{2}d\right)} \tag{2.18}$$

As an example we show the results for the case of metal backed chiral slab of thickness $d = 2$ mm at frequency 100 GHz (figure 2-1). The power reflection coefficients for TE and TM incidence are plotted as functions of the angle of incidence. The dielectric constant is taken $\epsilon = (5 + i0.1)\epsilon_0$ while the chirality β is varied from 0 to the order of 10^4. These cases are examined, among others, in [22].

As can be seen in the plots, in the case of real β the reflection coefficients are considerably lower than for an achiral lossy dielectric, while a complex β does not seem to contribute in the reduction of the reflection. In addition, chirality does not have any effect in reducing the reflection if the coating is lossless.

2.3   Chiral Slab in Air

Following the previous analysis, in the case of normal incidence, we can calculate the reflection and transmission coefficients for a chiral slab occupying the region $0 \le z \le d$ in free space. For a normally incident plane wave the reflected wave will be linearly polarized in the same direction, while the transmitted is elliptically polarized. Thus it has a copolarized and a crosspolarized component with respect to the incident wave. With the copolarized components are along the $x-$ direction, we have:

Incident wave:

$$\overline{E}^i = \hat{x}e^{ik_0 z} \tag{2.19}$$

$$\overline{H}^i = \hat{y}\frac{1}{\eta_0}e^{ik_0 z} \tag{2.20}$$

Reflected wave:

$$\overline{E}^r = \hat{x}Re^{-ik_0 z} \tag{2.21}$$

Power Reflection Coefficient

b=0.0 m
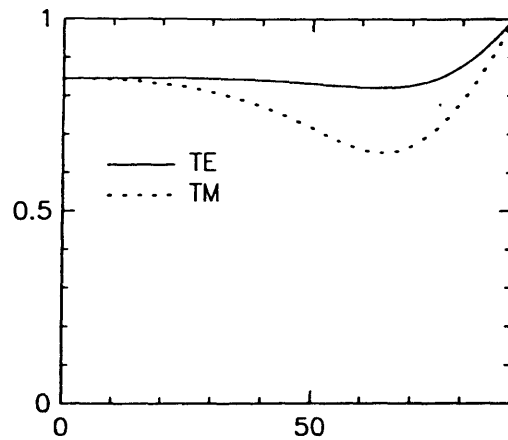
b=0.0002 m

b=0.0002(1+i) m

angle (deg)
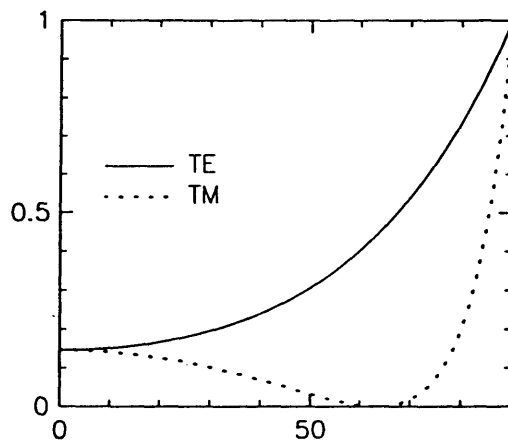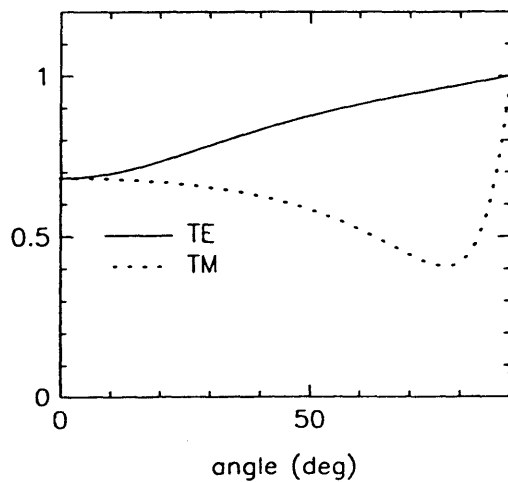
Figure 2-1: Reflection from metal backed dielectric slab

$$\overline{H}^r = \hat{y}\frac{1}{\eta_0}Re^{-ik_0 z} \qquad (2.22)$$

Transmitted wave:

$$\overline{E}^t = \hat{x}T_{co}e^{ik_0 z} + \hat{y}T_{cr}e^{ik_0 z} \qquad (2.23)$$

$$\overline{H}^t = \frac{1}{\eta_0}\left(\hat{y}T_{co}e^{ik_0 z} - \hat{x}T_{cr}e^{ik_0 z}\right) \qquad (2.24)$$

Eigenmodes in chiral slab:

$$\overline{Q}_{\substack{L \\ R}} = A_{\substack{L \\ R}}\left(\hat{x} \pm i\hat{y}\right)e^{ik_{\substack{L \\ R}}z} + B_{\substack{L \\ R}}\left(\hat{x} \mp i\hat{y}\right)e^{-ik_{\substack{L \\ R}}z} \qquad (2.25)$$

Fields in chiral slab:

$$\overline{E}_{ch} = \overline{Q}_L + a_R\overline{Q}_R \qquad (2.26)$$

$$\overline{H}_{ch} = a_L\overline{Q}_L + \overline{Q}_R \qquad (2.27)$$

Boundary conditions:

at z = 0:

$$\hat{x}\cdot\left(\overline{E}^i + \overline{E}^r - \overline{E}^{ch}\right) = 0 \qquad (2.28)$$

$$\hat{x}\cdot\left(\overline{H}^i + \overline{H}^r - \overline{H}^{ch}\right) = 0 \qquad (2.29)$$

$$\hat{y}\cdot\left(\overline{E}^i + \overline{E}^r - \overline{E}^{ch}\right) = 0 \qquad (2.30)$$

$$\hat{y}\cdot\left(\overline{H}^i + \overline{H}^r - \overline{H}^{ch}\right) = 0 \qquad (2.31)$$

at z = d:

$$\hat{x}\cdot\left(\overline{E}^{ch} - \overline{E}^t\right) = 0 \qquad (2.32)$$

$$\hat{x}\cdot\left(\overline{H}^{ch} - \overline{H}^t\right) = 0 \qquad (2.33)$$

$$\hat{y}\cdot\left(\overline{E}^{ch} - \overline{E}^t\right) = 0 \qquad (2.34)$$

$$\hat{y}\cdot\left(\overline{H}^{ch} - \overline{H}^t\right) = 0 \qquad (2.35)$$

Thus:

$$R = \frac{\eta^2 - \eta_0^2}{2\eta\eta_0 \cos(\frac{k_L + k_R}{2}d) - i(\eta^2 + \eta_0)\sin(\frac{k_L + k_R}{2}d)} \qquad (2.36)$$

and

$$T_{co} = T\cos(\frac{k_L - k_R}{2}d) \qquad (2.37)$$

$$T_{cr} = -T\sin(\frac{k_L - k_R}{2}d) \qquad (2.38)$$

where T_{co}, T_{cr} are the transmission coefficients for the copolarized and the crosspolarized components of the transmitted wave, respectively and

$$T = \frac{2\eta\eta_0}{2\eta\eta_0 \cos(\frac{k_L + k_R}{2}d) - i(\eta^2 + \eta_0)\sin(\frac{k_L + k_R}{2}d)} \qquad (2.39)$$

2.4 Reflection and Transmission Measurements

The theory for plane wave transmission and reflection serves as a basis for calculating the material parameters from measurements of the electromagnetic response of a chiral slab. The experimental data are usually in the form of complex reflection and transmission coefficients. For slab measurements at the normal incidence, it appears possible to find the material parameters by direct inversion of the reflection and transmission coefficients [5],[21].

As we have seen, the reflected and transmitted waves for a planar chiral sample are linearly and elliptically polarized, respectively for normally incident linearly polarized waves. Therefore, one reflection measurement is enough to describe the reflected field and two transmission measurements at different polarization angles are needed to fully determine the transmitted polarized wave. Thus, the transmission measurements can be broken down into two orthogonal components that are copolarized and crosspolarized, respectively, with respect to the incident linearly polarized plane wave. The real part of the chirality parameter can be determined through the angle of rotation θ between the polarization direction of the incident electric field and the direction of the major axis of the field polarization ellipse. On the other
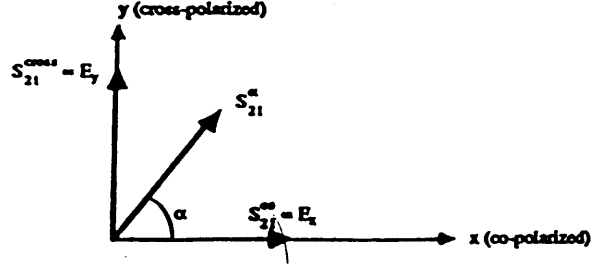
Figure 2-2: Components of transmitted wave

hand, the imaginary part of chirality is related to the ellipticity of the polarization ellipse. These angles can be determined if the transmitted field has been measured at two angles by rotating the receiving antenna, because these complex measurements determine the ellipse of the wave.

The S parameters are used to denote the reflection and transmission coefficients. S_{11} is the reflection coefficient, S_{21} is the transmission coefficient, while the subscripts co and cr are used again to denote the copolarized and crosspolarized components, respectively. The transmission at an arbitrary angle α with respect to incidence is denoted by S_{21_α}. Therefore (Figure 2-2):

$$S_{21_{cr}} = \frac{S_{21_\alpha} - S_{21_{co}} \cos \alpha}{\sin \alpha} \qquad (2.40)$$

Theoretically we can relate the S parameters for linearly polarized incident waves to those for LCP and RCP polarized waves in combination with (2.37), (2.38) using the relations:

$$S_{11} = S_{11_R} = S_{11_L} \qquad (2.41)$$

$$S_{21_R} = S_{21_{co}} + iS_{21_{cr}} = Te^{-i\frac{k_L - k_R}{2}d} \qquad (2.42)$$

$$S_{21_L} = S_{21_{co}} - iS_{21_{cr}} = Te^{i\frac{k_L - k_R}{2}d} \qquad (2.43)$$

$$\frac{S_{21_R}}{S_{21_L}} = e^{i(k_L - k_R)d} \qquad (2.44)$$

with $k_{L \atop R} = k'_{L \atop R} + ik''_{L \atop R}$. The Stokes parameters can be used to find the angle of

31
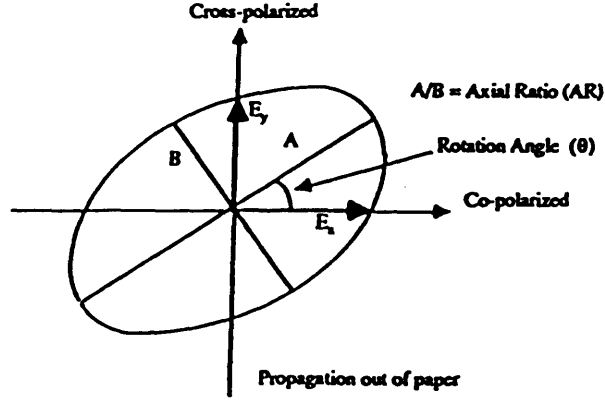
Figure 2-3: Polarization ellipse of transmitted wave showing rotation angle and axial ratio

rotation and the ellipticity of the polarization ellipse (Figure 2-3). Assuming that the polarization of the incident wave is in the x—direction it can be seen in Figure 2-2 that

$$S_{21_{co}} = E_x \tag{2.45}$$

$$S_{21_{cr}} = E_y \tag{2.46}$$

Therefore the Stokes parameters in combination with (2.37), (2.38) give:

$$S_0 = E_x E_x^* + E_y E_y^* = |T|^2 \cosh[(k_L'' - k_R'')d] \tag{2.47}$$

$$S_1 = E_x E_x^* - E_y E_y^* = |T|^2 \cos[(k_L' - k_R')d] \tag{2.48}$$

$$S_2 = -2\mathrm{Re}E_x E_y^* = |T|^2 \sin[(k_L' - k_R')d] \tag{2.49}$$

$$S_3 = 2\mathrm{Im}E_x E_y^* = |T|^2 \sinh[(k_L'' - k_R'')d] \tag{2.50}$$

The rotation angle θ can be found from (2.48), (2.49) as:

$$\theta = \frac{1}{2}\tan^{-1}\left(\frac{S_2}{S_1}\right) = \frac{k_L' - k_R'}{2}d \pm n\pi \tag{2.51}$$

The ambiguity for θ can be removed by another measurement with a different thickness sample which determines n.

The ellipticity ψ is related to the major axis A and the minor axis B of the ellipse

32

as:

$$\tan \psi = \frac{B}{A} \tag{2.52}$$

and can be found from (2.47), (2.50) is given by:

$$\psi = \frac{1}{2} \sin^{-1} \left(\frac{S_3}{S_0} \right) = \frac{1}{2} \sin^{-1} \{ \tanh[(k_L'' - k_R'')d] \} \tag{2.53}$$

The ellipticity can be measured through the axial ratio AR which is the ratio between the major axis and the minor axis of the ellipse and is therefore given by:

$$AR = \frac{1}{\tan \psi} \tag{2.54}$$

For the axial ratio we have: $1 \leq |AR| \leq \infty$, with 1 for circular polarization and ∞ for linear polarization. In general, $AR > 1$ corresponds to right elliptical polarization, while $AR < 1$ corresponds to left elliptical polarization.

From transmission measurements the real and imaginary parts of the chirality can be determined independently from the other two material parameters as can be seen in (2.51) and (2.53). On the other hand, we cannot determine the permittivity and permeability without knowing the chirality value. Provided that the chirality has been measured, the other two parameters can be determined from the reflection measurement combined with the copolarized transmission data. In the inversion algorithm there are again multiwavelength ambiguities expressed by integer numbers, and can be removed by repeating the measurement at another frequency or slab thickness.

The available experimental results for the electromagnetic properties of chiral composites that are used for comparison with the theoretical predictions are similar measurement procedures [25],[15].

33

Chapter 3

Modelling of Artificial Chiral Media

3.1 Introduction

When an electromagnetic wave propagates through an artificial medium it induces currents on the scatterers it includes. The scatterers can be viewed as equivalent electric and/or magnetic dipole moments that modify the net electric and/or magnetic dipole moments per unit volume, thus modifying the effective electromagnetic parameters of the medium [10]. An interesting and useful feature of artificial media is that by adjusting the size, shape and density of the scatterers it is possible to construct a medium with different electromagnetic properties.

For composite chiral media, the determination of the polarizability of the chiral inclusions is the first step in the modelling of heterogeneous complex materials in the case of weak mixtures. The polarizability components express the dielectric, magnetic and magnetoelectric responses of the inclusion element, and once these are known, it is possible to characterize mixtures that are composed of these inclusions embedded in a host medium using a quasistatic theory to derive mixing formulas involving the polarizabilities. The macroscopic parameters depend, in addition to the polarizabilities, on the fractional volumes of the components making the mixture. Since the analysis has been based on quasistatic assumptions, the mixing rules are

35

restricted by it. Therefore, the limitation of the formulas used so far is that the size of the inclusions has to be much smaller than the wavelength. A limit is that the size parameter $k_{eff}d$ is less than 1, where d is the average diameter of the particle and k_{eff} is the wave number within the mixture [9].

3.2   Standard Maxwell-Garnett Mixing Formula

The simplest mixing rule is the Maxwell-Garnett formula which gives the effective permittivity ϵ_{eff} of a dielectric medium where spheres of permittivity ϵ occupy a volume fraction f in a host medium of permittivity ϵ_0 :

$$\epsilon_{eff} = \epsilon_0 + 3f\epsilon_0 \frac{\epsilon - \epsilon_0}{\epsilon + 2\epsilon_0 - f(\epsilon - \epsilon_0)} \tag{3.1}$$

The Maxwell-Garnett formula can be derived from the following independencies. The effective permittivity gives the relation between the electric field and the average electric flux density:

$$\langle \overline{D} \rangle = \epsilon_{eff}\overline{E} = \epsilon_0\overline{E} + \langle \overline{P_e} \rangle \tag{3.2}$$

The average polarization is the dipole moment density:

$$\langle \overline{P_e} \rangle = n_0 \overline{p}_e \tag{3.3}$$

where n_0 is the number density of the electric dipoles. The electric dipoles are determined by the electric polarizability α and the field exciting the inclusions: $\overline{p}_e = \alpha \overline{E}^L$. The exciting field $\overline{E}^L$ also called Lorentzian field, is larger than the average field $\overline{E}$ because it includes the contribution from the surrounding polarization:

$$\overline{E}^L = \overline{E} + \frac{\overline{P}_e}{3\epsilon_0} \tag{3.4}$$

36

The combination of these conditions yields the dielectric mixing rule. The effective permittivity in terms of the polarizability, is given by the Lorenz-Lorentz formula.

$$\epsilon_{eff} = \epsilon_0 + \frac{n_0\alpha}{1 - \frac{n_0\alpha}{3\epsilon_0}} \tag{3.5}$$

3.3   Chiral Maxwell-Garnett Mixing Formula

Using an extension of the standard Maxwell-Garnett mixing formula to the case of an effective chiral medium [7], the effective electromagnetic parameters that appear in the macroscopic constitutive relations, can be expressed in terms of the polarizabilities of the chiral particles embedded in the host medium. This mixing law is based on the quasistatic analysis of scattering by a chiral sphere and is therefore valid at low frequencies. So the assumptions made in this approach are:

- The inclusions are spherical chiral particles

- The size of the inclusions is small compared to wavelength

- The spheres are non-interactive.

Consider a mixture made up of an achiral background with permittivity ϵ_0 and permeability μ_0 which includes n_0 spherical chiral scattteres per unit volume. The composite medium is described by the constitutive relations of an effective chiral medium:

$$\langle \overline{D} \rangle = \epsilon_{eff}\overline{E} + i\kappa_{eff}\sqrt{\mu_0\epsilon_0}\,\overline{H} \tag{3.6}$$

$$\langle \overline{B} \rangle = \mu_{eff}\overline{H} - i\kappa_{eff}\sqrt{\mu_0\epsilon_0}\,\overline{E} \tag{3.7}$$

Also:

$$\langle \overline{D} \rangle = \epsilon_0\overline{E} + \langle \overline{P}_{ee} \rangle + \langle \overline{P}_{em} \rangle \tag{3.8}$$

$$\langle \overline{B} \rangle = \mu_0\overline{H} + \langle \overline{P}_{me} \rangle + \langle \overline{P}_{mm} \rangle \tag{3.9}$$

37

where $\overline{P}_{ee}$ and $\overline{P}_{em}$ are the electric dipole moments per unit volume induced by the electric and the magnetic field, respectively, while $\overline{P}_{me}$ and $\overline{P}_{mm}$ are the magnetic dipole moments per unit volume induced by the electric and the magnetic field, respectively. These are related to the dipole moments of a single scatterer as:

$$\langle \overline{P}_{ij} \rangle = n_0 \overline{p}_{ij} \tag{3.10}$$

where i, j denote any combination of e and m. The dipole moments are proportional to the exciting (Lorentzian) fields:

$$\overline{p}_{\xi e} = \alpha_{\xi e} \overline{E}^L \tag{3.11}$$

$$\overline{p}_{\xi m} = \alpha_{\xi m} \overline{H}^L \tag{3.12}$$

where $\alpha_{\xi e}$ and $\alpha_{\xi m}$ are the polarizabilities of the scatterer and ξ is either e or m. The exciting fields $\overline{E}^L$ and $\overline{H}^L$ are given by the quasistatic analysis of scattering from a sphere, in terms of the average fields $\overline{E}$ and $\overline{H}$ as:

$$\overline{E}^L = \overline{E} + \frac{\overline{P}_e}{3\epsilon_0} \tag{3.13}$$

$$\overline{H}^L = \overline{H} + \frac{\overline{P}_m}{3\mu_0} \tag{3.14}$$

Using the relations (3.10), (3.11) and (3.12), the total electric and magnetic dipole moments per unit volume $\overline{P}_e$ and $\overline{P}_m$, respectively, can be written as:

$$\overline{P}_e = n_0 \alpha_{ee} \overline{E}^L + n_0 \alpha_{em} \overline{H}^L \tag{3.15}$$

$$\overline{P}_m = n_0 \alpha_{me} \overline{E}^L + n_0 \alpha_{mm} \overline{H}^L \tag{3.16}$$

$$\tag{3.17}$$

and in combination with (3.13) and (3.14) we get:

$$\left(1 - \frac{n_0 \alpha_{ee}}{3\epsilon_0}\right) \overline{P}_e - \frac{n_0 \alpha_{em}}{3\mu_0} \overline{P}_m = n_0 \alpha_{ee} \overline{E} + n_0 \alpha_{em} \overline{H} \tag{3.18}$$

38

$$-\frac{n_0\alpha_{me}}{3\epsilon_0}\overline{P}_e + \left(1 - \frac{n_0\alpha_{mm}}{3\mu_0}\right)\overline{P}_m = n_0\alpha_{me}\overline{E} + n_0\alpha_{mm}\overline{H} \qquad (3.19)$$

Solving the system of 3.18, 3.19 for $\overline{P}_e$ and $\overline{P}_m$ in terms of the fields and the polarizabilities, the following expressions for the effective parameters are derived:

$$\epsilon_{eff} = \epsilon_0 + \frac{(1 - n_0\alpha_{mm}/3\mu_0)\,n_0\alpha_{ee} + n_0^2\alpha_{em}\alpha_{me}/3\mu_0}{A} \qquad (3.20)$$

$$\mu_{eff} = \mu_0 + \frac{(1 - n_0\alpha_{ee}/3\epsilon_0)\,n_0\alpha_{mm} + n_0^2\alpha_{em}\alpha_{me}/3\epsilon_0}{A} \qquad (3.21)$$

$$\kappa_{eff} = -\frac{i}{\sqrt{\mu_0\epsilon_0}}\frac{n_0\alpha_{em}}{A} = \frac{i}{\sqrt{\mu_0\epsilon_0}}\frac{n_0\alpha_{me}}{A} \qquad (3.22)$$

where

$$A = (1 - n_0\alpha_{ee}/3\epsilon_0)\,(1 - n_0\alpha_{mm}/3\mu_0) - n_0^2\alpha_{em}\alpha_{me}/9\mu_0\epsilon_0$$

Using the expressions for the polarizabilities as given by the quasistatic analysis of scattering from a chiral sphere with radius a, permittivity ϵ, permeability μ and chirality κ [8]:

$$\alpha_{ee} = 4\pi a^3\epsilon_0\frac{(\mu + 2\mu_0)(\epsilon - eps_0) - \kappa^2\mu_0\epsilon_0}{B} \qquad (3.23)$$

$$\alpha_{em} = 4\pi a^3\sqrt{\mu_0\epsilon_0}\frac{i3\kappa\mu_0\epsilon_0}{B} \qquad (3.24)$$

$$\alpha_{mm} = 4\pi a^3\mu_0\frac{(\mu - \mu_0)(\epsilon + 2eps_0) - \kappa^2\mu_0\epsilon_0}{B} \qquad (3.25)$$

$$\alpha_{me} = 4\pi a^3\sqrt{\mu_0\epsilon_0}\frac{-i3\kappa\mu_0\epsilon_0}{B} \qquad (3.26)$$

with $B = (\mu + 2\mu_0)(\epsilon + 2\epsilon_0) - \kappa^2\mu_0\epsilon_0$, equations (3.20), (3.21) and (3.22) become:

$$\epsilon_{eff} = \epsilon_0 + 3f\epsilon_0\frac{(\epsilon - \epsilon_0)[(\mu + 2\mu_0) - f(\mu - \mu_0)] - \kappa^2\mu_0\epsilon_0(1 - f)}{C} \qquad (3.27)$$

$$\mu_{eff} = \mu_0 + 3f\mu_0\frac{(\mu - \mu_0)[(\epsilon + 2\epsilon_0) - f(\epsilon - \epsilon_0)] - \kappa^2\mu_0\epsilon_0(1 - f)}{C} \qquad (3.28)$$

$$\kappa_{eff} = \frac{9f\kappa\mu_0\epsilon_0}{C} \qquad (3.29)$$

where f is the fractional volume of the chiral inclusion phase of the mixtures and $C = [(\mu + 2\mu_0) - f(\mu - \mu_0)][(\epsilon + 2\epsilon_0) - f(\epsilon - \epsilon_0)] - \kappa^2\mu_0\epsilon_0(1 - f)^2$.

It is easy to check that the above mixing rules satisfy all the requirements saddled on a tentative mixing formula:

- for $f = 0$, the permittivity and the permeability are those of the background medium while the chirality vanishes

- for $f = 1$, the effective parameters are those of the inclusion phase

- if the chirality of the inclusion phase vanishes, the effective chirality vanishes

  and the formulas reduce to the standard Maxwell-Garnett mixing formula

One impressive aspect about the chiral Maxwell-Garnett mixing formulas is the set of multiple dualities in the macroscopic expressions: The way the permittivity ϵ of the inclusions affects the effective permittivity ϵ_{eff}, chirality κ_{eff} and permeability μ_{eff} is the same as the way the permeability μ of the inclusions affects the effective permeability μ_{eff}, chirality κ_{eff} and permittivity ϵ_{eff}.

It is important to observe that the effective permittivity and permeability of a mixture are even functions of the chirality of the inclusion phase. Hence the sign of handedness should not have effect on these parameters, and they are scalars, invariant of space inversion. This is because samples of media that are mirror images of one another should have the same permittivity and the same permeability. Although in the subatomic level, in the weak interaction process, the asymmetry between left and right has been predicted and experimentally observed one should expect this not to happen at the macroscopic level where racemization processes tend to eliminate handed effects [9].

The effective chirality parameter is an odd function of the chirality of the inclusions. A change in the handedness of the component changes the handedness of the mixture.

3.4   Conclusion

Both standard and chiral Maxwell-Garnett formulas are limited to low frequencies. That is, the scatterers must be sufficiently small compared to the wavelength, so

that quasistatics can apply. The Mawell-Garnett mixing law is also valid only for low inclusions since it ignores the scattering loss which becomes important at higher concentrations.

This approach under the assumptions made above can be applicable to the case of chiral particles of any shape, for example miniature helices. Since the scattering behavior is strongly dependent on the size of the particles, objects with dimensions comparable to the wavelength require more complicated treatment than small inclusions, and the Maxwell-Garnett formula is no longer accurate.

Chapter 4

Electromagnetic Properties of Helix Loaded Composites

4.1 Introduction

Helices are perhaps the most common chiral (handed) objects found in nature. A helix can be either left-handed or right-handed (Figure 4-1). The one turn helix is the canonical three-dimensional chiral structure [18]. A helical wire on a uniform cylinder becomes a straight wire when unwound by rolling the cylinder on a flat surface. Viewed end-on, a helix projects as a circle. Thus, a helix combines the geometric forms of a straight wire, a cylinder and a circle. The dimensions of a helix are conveniently represented by either pitch P and circumference C, or the length of one turn L and the pitch angle α. When the pitch is zero then $\alpha = 0^o$ and the helix becomes a loop. When the diameter is zero then $\alpha = 90^o$ and the helix becomes a linear conductor. It is noted that there is no chirality when $\alpha = 0^o$ or $\alpha = 90^o$ because, in these two limits, there is no handedness.

The magnetoelectric coupling can be intuitively grasped from the behavior of a helix as it is exposed to the electromagnetic field. If an electric field excites the helix, it separates charges, creating an electric dipole moment. This contributes to the permittivity of the composite medium, but the shape of the helix forces the charge to move along a circular route, in addition to the linear path. This electric current loop
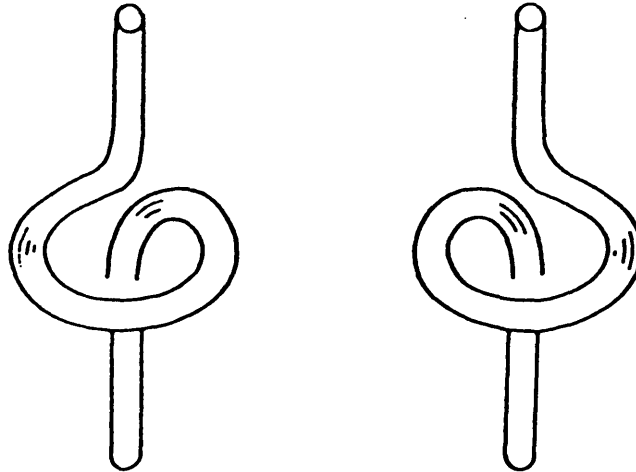
Figure 4-1: Left-handed and right-handed one turn helix

is equivalent to a magnetic dipole, and if all the helices in a mixture have the same handedness, the magnetic polarization effect will be enhanced. The corresponding appearance of both types of both types of polarization results also for magnetic field excitation.

It is interesting to study what is the electromagnetic effect on a given left-handed or right-handed structure. A specific helix should scatter differently to an incident left-handed wave compared to a right-handed wave. The objective is to predict the effective permittivity, permeability and chirality of a medium, knowing the dimensions and the concentration of helices embedded in the sample.

To secure isotropy, helices must be randomly oriented so that there is no preferred direction (Figure 4-2a). If the helices are set in arrays in alligned configuration the result is a macroscopically bianisotropic material, leading to dyadic (or matrix) coefficients in the constitutive relations (Figure 4-2b).

In practice, any method of making an artificial chiral medium will affect all the medium parameters (dielectric, magnetic and chiral), together. Thus to investigate

44
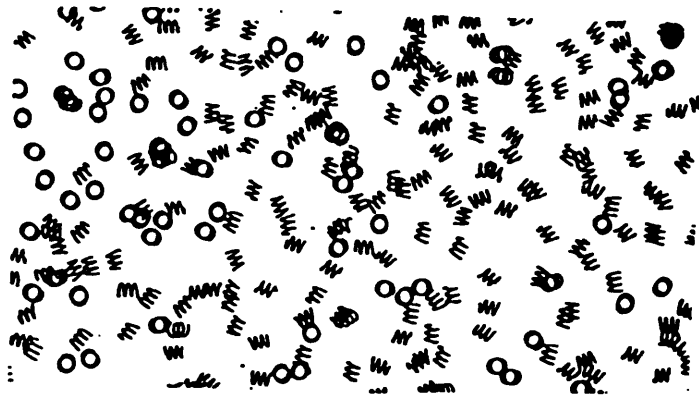
(a)
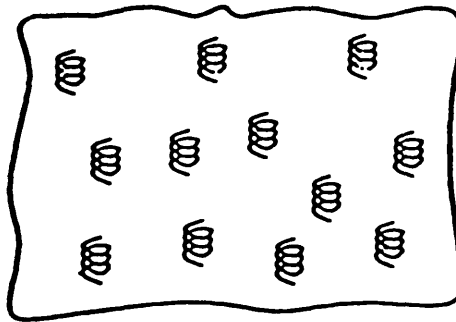
(b)

Figure 4-2: Samples of artificial chiral material (a) isotropic (b) anisotropic

the possible effects, one must start from detailed analysis of the chiral objects. We then include all the effects of the actually adjustable physical parameters, rather than varying a chirality which cannot be independedly adjusted. Such an analysis is performed here for a chiral composite medium containing metal wire helices, which have been used in many published works. The electric and magnetic moments of the helix are calculated using the method of moments. These are then used to find the electromagnetic properties of the composite medium using the Maxwell-Garnett mixing for effective chiral media.

4.2 Scattering from Helix

Starting from the study by Jaggard et al. [6] there has been work on a quasistatic approach to the modelling of helix scattering. In these investigations the polarizabilities of the helix are calculated as functions of the static capacitance and inductance of the straight portion and loop of the helix, and the crosspolarizabilities are connected with the copolarizabilities. As the polarizability matrix elements are known, the effective parameters can also be calculated using some mixing formula. The problem with the early models has been the narrowband character of their validity around the resonant frequency of the helix.

To attack the electromagnetic problem involving chiral geometries, one needs to write boundary conditions on handed surfaces. The formulation of these conditions on a helix surface leads to a problem with greater analytical difficulties than in the corresponding nonchiral geometries. Therefore no analytical solutions for the helix scattering problem exist. However, numerical and approximate efforts in the literature are numerous [3].

4.2.1 Formulation

The currents induced on a helix are calculated, using a method of moments (Galerkin's method) to solve the electric field integral equation (EFIE) under a thin wire approximation. In order to use a thin wire approximation, the wires under consideration are

assumed to be thin with uniform radius and with diameter less than 0.01λ [27].

We consider first the case of perfectly conducting wires. Integral equations for conducting wire structures can generally be written in terms of the following statement of a boundary condition on the surface of the wire.

$$\hat{n} \cdot \nabla \times \left(\overline{E}^i + \overline{E}^s\right) = 0 \qquad (4.1)$$

where $\hat{n}$ is the unit vector normal to the wire surface, $\overline{E}^i$ and $\overline{E}^s$ are the incident and scattered fields, respectively. A more useful form for this case is:

$$\hat{l} \cdot \left(\overline{E}^i + \overline{E}^s\right) = 0 \qquad (4.2)$$

where $\hat{l}$ is the unit vector tangential to the wire surface.

In thin problems the surface and volume integrals representing the scattered field are approximated by simpler linear integrals that can circumvent the difficulty of source singularity in the self elements (usually the diagonal terms) of the matrix equation. In a thin wire wire structure with wire radius a, both the electric field and the surface current density $\overline{J}_S$ on the surface S have essentially only one axial component along the wire axis l. $\overline{E}^s$ and $\overline{J}_S$ are also approximately uniform in phase and amplitude around the circumferance C. Thus, the fields on S due to $\overline{J}_S$ can be approximated by the fields due to an equivalent axial current I_l given by:

$$\overline{I}_l(l') = \hat{l}'I(l') \simeq \hat{l}'2\pi a J_S(\overline{r}') \simeq 2\pi a \overline{J}_S(\overline{r}') \qquad (4.3)$$

The above expression is valid under the following assumptions:

- Only the component of the surface current along the helical tangent contributes to the scattered field.

- The surface current along the helical tangent is uniformly disrtibuted around the wire perimeter.

- The electric field in the vicinity of the wire is quasi-static in nature so the current

can be assumed to be concentrated at the center of the wire without altering the

fields outside the cylindrical surface.

The composite medium of interest, is made up of identical randomly oriented helices embedded in a host medium with background parameters ϵ_0 and μ_0. Each helix has N turns, radius b, wire radius a, pitch P and axis along z-direction (Figure 4-3). The total length L of a helix is then:

$$L = 2\pi\sqrt{b^2 + \left(\frac{P}{2\pi}\right)^2} \tag{4.4}$$

The position vectors on the wire axis and on the wire surface respectively are [3]:

$$\bar{r}' = b\cos\phi'\hat{x} + b\sin\phi'\hat{y} + \frac{P}{2\pi}\phi'\hat{z} \tag{4.5}$$

$$\bar{r} = (a+b)\cos\phi\hat{x} + (a+b)\sin\phi\hat{y} + \frac{P}{2\pi}\phi\hat{z} \tag{4.6}$$

and the tangential unit vectors along the wire axis and the wire surface are [3]:

$$\hat{t}'(\phi') = \frac{1}{t}\left(-b\sin\phi'\hat{x} + b\cos\phi'\hat{y} + \frac{P}{2\pi}\hat{z}\right) \tag{4.7}$$

$$\hat{t}(\phi) = \frac{1}{s}\left[-(a+b)\sin\phi\hat{x} + (a+b)\cos\phi\hat{y} + \frac{P}{2\pi}\hat{z}\right] \tag{4.8}$$

where

$$t = \sqrt{b^2 + (P/2\pi)^2} \tag{4.9}$$

$$s = \sqrt{(a+b)^2 + (P/2\pi)^2} \tag{4.10}$$

with $0 \leq \phi \leq \Phi$ and $\Phi = 2\pi N$. The scattered electric field is given by the electric field integral equation:

$$\bar{E}^s = i\omega\mu_0 \iint_S \left|d\bar{S}'\right| \overline{\overline{G}}(\bar{r},\bar{r}')\bar{J}_S(\bar{r}') \tag{4.11}$$
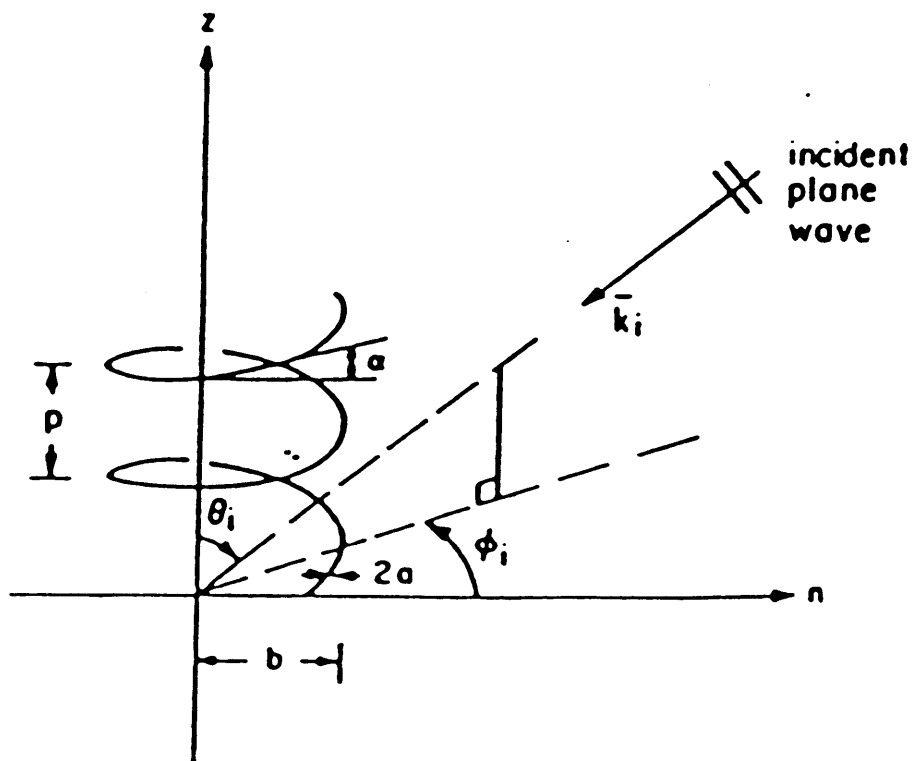
48

Figure 4-3: Thin helical wire

which in the thin wire approximation takes the form:

$$\bar{E}^s = i\omega\mu_0 \int_L |d\bar{r}'| \, \bar{\bar{G}}(\bar{r}, \bar{r}') \bar{I}(\bar{r}') \tag{4.12}$$

where:

$$\bar{\bar{G}}(\bar{r}, \bar{r}') = \left(\bar{\bar{I}} + \frac{1}{k_0^2} \nabla\nabla \right) g(\bar{r}, \bar{r}') \tag{4.13}$$

is the dyadic Green's function and $k_0 = \omega\sqrt{\mu_0\epsilon_0}$.

$$g(\bar{r}, \bar{r}') = \frac{e^{ik_0|\bar{r}-\bar{r}'|}}{4\pi|\bar{r} - \bar{r}'|} = \frac{e^{ik_0 R}}{4\pi R} \tag{4.14}$$

is the scalar Green's function and

$$R = \sqrt{\rho^2 + \rho'^2 - 2\rho\rho' \cos v + (P/2\pi)^2 v^2} \tag{4.15}$$

is the distance from the source to the observation point and $v = \phi - \phi'$. The induced current is along the wire axis, so:

$$\bar{I} = \hat{t}'(\phi')I(\phi') \tag{4.16}$$

$$|d\bar{r}'| = t d\phi' \tag{4.17}$$

and equation (4.12) takes the form:

$$\bar{E}^s = i\eta_0 k_0 t \int_0^\Phi d\phi' \bar{\bar{G}}(\bar{r}, \bar{r}') \hat{t}'(\phi')I(\phi') \tag{4.18}$$

where $\eta_0 = \sqrt{\mu_0/\epsilon_0}$. If the helix is perfectly conducting then the boundary condition (4.2) on its surface is:

$$\hat{t}(\phi) \cdot (\bar{E}^i + \bar{E}^s) = 0 \tag{4.19}$$

which, in combination with equations (4.13) and (4.18) gives:

$$-\hat{t}(\phi) \cdot \overline{E}^i = i\eta_0 k_0 t \hat{t}(\phi) \int_0^\Phi d\phi' \left[\hat{t}(\phi) \cdot \hat{t}'(\phi') + \frac{1}{k_0^2}(\hat{t}(\phi) \cdot \nabla)(\hat{t}'(\phi')\nabla)\right] g(\phi, \phi')I(\phi') \tag{4.20}$$

With the following manipulations we can derive from (4.20), an expression depending only on the difference $v = \phi - \phi'$:

$$\frac{\partial g}{\partial \phi} = \frac{\partial g}{\partial v} \tag{4.21}$$

$$\hat{t}(\phi) \cdot \hat{t}'(\phi') = \frac{1}{st}\left[b(a+b)\cos v + \left(\frac{P}{2\pi}\right)^2\right] \tag{4.22}$$

$$\hat{t}(\phi) \cdot \nabla g = \frac{1}{s}\left(\frac{\partial g}{\partial v} + \frac{P}{2\pi}\frac{\partial g}{\partial z}\right) \tag{4.23}$$

$$\hat{t}'(\phi') \cdot \nabla g = \frac{1}{t}\left(b\sin v\frac{\partial g}{\partial \rho} + \frac{b}{a+b}\cos v\frac{\partial g}{\partial v} + \frac{P}{2\pi}\frac{\partial g}{\partial z}\right) \tag{4.24}$$

But:

$$\frac{\partial g}{\partial \rho} = \frac{\partial f}{\partial \rho}\frac{dg}{df} = [2(a+b) - 2b\cos v]\frac{dg}{df} \tag{4.25}$$

$$\frac{\partial g}{\partial \phi} = \frac{\partial f}{\partial \phi}\frac{dg}{df} = 2b(a+b)\sin v\frac{dg}{df} \tag{4.26}$$

where

$$f = \rho^2 + \rho'^2 - 2\rho\rho'\cos v + \left(\frac{P}{2\pi}\right)^2 v^2 \tag{4.27}$$

Combining (4.25) and (4.26) gives:

$$b\sin v\frac{\partial g}{\partial \rho} = \frac{a+b-b\cos v}{a+b}\frac{\partial g}{\partial v} \tag{4.28}$$

Thus:

$$\hat{t}'(\phi') \cdot \nabla g = \frac{1}{t}\left(\frac{\partial g}{\partial v} + \frac{P}{2\pi}\frac{\partial g}{\partial z}\right) \tag{4.29}$$

51

and because:

$$\frac{dg}{dv} = \frac{\partial g}{\partial v} + \frac{dz}{dv}\frac{\partial g}{\partial z} \tag{4.30}$$

equations (4.23) and (4.24) become:

$$\hat{t}(\phi) \cdot \nabla g = \frac{1}{s}\frac{dg}{dv} \tag{4.31}$$

$$\hat{t}'(\phi') \cdot \nabla g = \frac{1}{t}\frac{dg}{dv} \tag{4.32}$$

and equation (4.20) can take the following final form:

$$- s\hat{t}(\phi) \cdot \overline{E}^i(\phi) = \frac{i\eta_0}{4\pi k_0} \int_0^\Phi d\phi' K(\phi - \phi')I(\phi') \tag{4.33}$$

where:

$$K(v) = \left[k_0^2(a+b)b\cos v + \left(\frac{k_0 P}{2\pi}\right)^2 + \frac{d^2}{dv^2} \right] \frac{e^{ik_0 R}}{R} \tag{4.34}$$

4.2.2 Method of Moments

Using Galerkin's method, the integral equation (4.33) is discretized and converted into a set of linear equations by expanding the induced current into a set of basis functions $f_n(\phi)$ and testing the equation at a number of points with $f_n(\phi)$ as testing function. The general guideline for the discretization procedure is that the length of each segment should not exceed $\lambda/4$ and that each segment should be less than approximately 100 times the shortest segment [27]. The induced current is expanded as:

$$I(\phi) = \sum_{n=1}^N I_n f_n(\phi) \tag{4.35}$$

where I_n are constants to be calculated and the resulting matrix equation is:

$$V_m = \sum_{n=1}^N Z_{mn} I_n \tag{4.36}$$

52

with:

$$V_m = \int_{D_m} d\phi \left[-s\hat{t}(\phi)\overline{E}^i(\phi) \right] f_m(\phi) \tag{4.37}$$

$$Z_{mn} = \frac{i\eta_0}{4\pi k_0} \int_{D_m} d\phi \int_{D_n} d\phi' K(\phi - \phi') f_n(\phi') f_m(\phi) \tag{4.38}$$

$$\tag{4.39}$$

and D_n is the interval $[\phi_{n-1}, \phi_{n+1}]$ where the function f_n is non-zero. In the case of finite conductivity the boundary condition on the helix surface under the thin wire approximation is:

$$\hat{t}(\phi) \cdot (\overline{E}^i + \overline{E}^s) = Z_s J_s = Z_s \frac{I(\phi)}{2\pi a} \tag{4.40}$$

where Z_s is the surface resistance of the wire. An approximate expression that we use for Z_s in this problem is [27]:

$$Z_s = \frac{T}{\sigma} \frac{J_0(Ta)}{J_1(Ta)} \tag{4.41}$$

where $T = i\omega\mu_0(\sigma - i\omega\epsilon_0)$, σ is the conductivity of the wire and J_0 and J_1 are Bessel functions of order 0 and 1, respectively. Galerkin's method is also applied in the case of finite conductivity. In our problem we choose triangular basis and testing functions which provide zero currents at the ends of the helix.

The dependence of the integrand on the difference $\phi - \phi'$ allows a reduction of the double integral of (4.38) to a single integral thus accelerating the process. The following transformation is applied [3]:

$$v = \phi - \phi' - (\phi_m - \phi_n)$$

$$u = \phi + \phi' - (\phi_m + \phi_n)$$

so that (4.38) becomes:

$$Z_{mn} = \frac{i\eta_0}{8\pi k_0} \int_{-2\Delta}^{2\Delta} dv \int_{-2\Delta-|v|}^{2\Delta+|v|} du K(v + \phi_m - \phi_n) f_n(\frac{u-v}{2} + \phi_n) f_m(\frac{u+v}{2} + \phi_m) \tag{4.42}$$

53

where $\Delta = \phi_n - \phi_{n-1}$.

The integral with respect to u can be found analytically so finally:

$$Z_{mn} = \frac{i\eta_0}{8\pi k_0} \int_{-2\Delta}^{2\Delta} dv \, [h_{mn}(v)T(v) + T''(v)] \frac{e^{ik_0 R_{mn}(v)}}{R_{mn}(v)} \qquad (4.43)$$

where

$$R_{mn}(v) = R(v + \phi_m + \phi_n)$$

$$h_{mn}(v) = k_0^2 b(a+b)\cos(v + \phi_m + \phi_n) + \left(\frac{k_0 P}{2\pi}\right)^2$$

$$T(v) = \begin{cases} \Delta\left(\frac{4}{3} - 2\left|\frac{v}{\Delta}\right|^2 + \left|\frac{v}{\Delta}\right|^3\right), & |v| \le \Delta \\[2ex] \Delta\left(\frac{8}{3} - 4\left|\frac{v}{\Delta}\right| + 2\left|\frac{v}{\Delta}\right|^2 - \frac{1}{8}\left|\frac{v}{\Delta}\right|^3\right), & |v| \ge \Delta \end{cases}$$

In order to get chirality in a helix loaded composite medium, the helices must be excited by an incident wave. The interaction between the helices and the electromagnetic excitation is expected to induce a non negligible chirality. The excitation of one helix can be considered as most efficient if the backscattered field absolute value is maximum. The pitch to ratio diameter appears as a relevant parameter for the excitation efficiency. The chiral efficiency of the helix is evaluated by the ratio between the crosspolarized and the copolarized backscatterded field and is also dependent on the helix parameters.

4.2.3 Helix Polarizabilities

Macroscopic modelling of chiral media requires the analysis of the response of the chiral inclusions in an electromagnetic field. The response can be described through the polarizability coefficients. Once these are known, the electromagnetic parameters of the material can be found.

Having found the induced currents on the helix, the next step is the calculation

of the equivalent dipole moments using the relations:

$$\overline{p}_e \;=\; \frac{i}{\omega} \int_L ds \overline{I}(s) \tag{4.44}$$

$$\overline{p}_m \;=\; \mu_0 \overline{m} = \frac{\mu_0}{2} \int_L ds \left[\overline{r}(s) \times \overline{I}(s) \right] \tag{4.45}$$

and in combination with the relations:

$$\overline{p}_e \;=\; \alpha_{ee} \overline{E}^i + \alpha_{em} \overline{H}^i \tag{4.46}$$

$$\overline{p}_m \;=\; \alpha_{me} \overline{E}^i + \alpha_{mm} \overline{H}^i \tag{4.47}$$

$$\tag{4.48}$$

the polarizabilities of a single helix can be obtained easily if we separate the excitations. This can be done by exciting the helix with two identical plane waves propagating in opposite directions so that in every case the fields (electric for the electric dipole moments and magnetic for the magnetic dipole moments) whose contribution we want to find, add, giving a uniform static field while the others cancel.

For a helix the expressions (4.44) and (4.45) for the dipole moments are:

$$\overline{p}_e \;=\; \frac{i}{\omega} \int_0^\Phi d\phi' t \hat{t}'(\phi') I(\phi') \tag{4.49}$$

$$\overline{p}_m \;=\; \frac{\mu_0}{2} \int_0^\Phi d\phi' t \overline{r}(\phi') \times \hat{t}'(\phi') I(\phi') \tag{4.50}$$

$$\tag{4.51}$$

Using the expressions (4.5), (4.7) and (4.16), (4.17) as well as (4.35) we have:

$$I(s) = \hat{t}(\phi) I(\phi) = \left[-b\sin(\phi)\hat{x} + b\cos(\phi)\hat{y} + \frac{P}{2\pi}\hat{z} \right] \sum_{n=1}^N I_n f_n(\phi) \tag{4.52}$$

thus:

$$\overline{p}_e = p_{e_x}\hat{x} + p_{e_y}\hat{y} + p_{e_z}\hat{z} \tag{4.53}$$

55

where:

$$p_{e_x} = -\frac{bi}{\omega} \sum_{n=1}^{N} I_n \int_{D_n} d\phi' \sin \phi' f_n(\phi') \tag{4.54}$$

$$p_{e_y} = \frac{bi}{\omega} \sum_{n=1}^{N} I_n \int_{D_n} d\phi' \cos \phi' f_n(\phi') \tag{4.55}$$

$$p_{e_z} = \frac{Pi}{2\pi\omega} \sum_{n=1}^{N} I_n \int_{D_n} d\phi' f_n(\phi') \tag{4.56}$$

and

$$\bar{p}_m = p_{m_x}\hat{x} + p_{m_y}\hat{y} + p_{m_z}\hat{z} \tag{4.57}$$

where:

$$p_{m_x} = \frac{\mu_0 bP}{4\pi} \sum_{n=1}^{N} I_n \int_{D_n} d\phi' \left(\sin \phi' - \phi' \cos \phi'\right) f_n(\phi')$$

$$p_{m_y} = \frac{\mu_0 bP}{4\pi} \sum_{n=1}^{N} I_n \int_{D_n} d\phi' \left(\cos \phi' + \phi' \sin \phi'\right) f_n(\phi')$$

$$p_{m_z} = \frac{\mu_0 b^2}{2} \sum_{n=1}^{N} I_n \int_{D_n} d\phi' f_n(\phi') \tag{4.58}$$

and can be calculated analytically since the coefficients I_n have been found.

For a helix, the polarizability is actually a tensor:

$$[\alpha_{ij}] = \begin{bmatrix} \alpha_{ij_{xx}} & \alpha_{ij_{xy}} & \alpha_{ij_{xz}} \\ \alpha_{ij_{yx}} & \alpha_{ij_{yy}} & \alpha_{ij_{yz}} \\ \alpha_{ij_{zx}} & \alpha_{ij_{zy}} & \alpha_{ij_{zz}} \end{bmatrix} \tag{4.59}$$

where again i, j denote any combination of e and m.

Averaging over orientation and spin of helix, the off-diagonal terms vanish so only $\alpha_{ij_{xx}}, \alpha_{ij_{yy}}, \alpha_{ij_{zz}}$ survive, and the average polarizability is:

$$\alpha_{ij} = \frac{\alpha_{ij_{xx}} + \alpha_{ij_{yy}} + \alpha_{ij_{zz}}}{3} \tag{4.60}$$

The averaging is done by keeping the exciting field fixed along a certain direction while the orientation of the helix and its spin are changed using the appropriate

56

tranformation matrix. First we vary the orientation of the helix. The new coordinate system (x', y', z') with the helix axis along the z'-axis is related to the initial coordinate system (x, y, z) through the transformation matrix T:

$$[T] = \begin{bmatrix} \cos\phi & \cos\theta\sin\phi & \sin\theta\cos\phi \\ -\sin\phi & \cos\theta\cos\phi & \sin\theta\sin\phi \\ 0 & -\sin\theta & \cos\theta \end{bmatrix} \qquad (4.61)$$

Thus, if $\bar{a}$ is a vector in the coordinate system (x, y, z) and $\bar{a}'$ the same vector in the new coordinate system (x', y', z') then:

$$\bar{a} = [T]\bar{a}' \qquad (4.62)$$

Next we vary the spin of the helix by rotation around its axis which stays fixed along the z'-axis. The new coordinate system (x'', y'', z'') is related to the coordinate system (x', y', z') through the transformation matrix T':

$$[T'] = \begin{bmatrix} \cos\gamma & \sin\gamma & 0 \\ -\sin\gamma & \cos\gamma & 0 \\ 0 & 0 & 1 \end{bmatrix} \qquad (4.63)$$

Thus, if $\bar{a}$ is a vector in the coordinate system (x, y, z), $\bar{a}'$ the same vector in the coordinate system (x', y', z') and $\bar{a}''$ in (x'', y'', z'') then:

$$\bar{a} = [T]\bar{a}' = [T][T']\bar{a}'' \qquad (4.64)$$

If for example the excitation field is polarized along the z-direction: $\overline{E} = \hat{z}E_0$ we have:

$$\overline{E} = \begin{bmatrix} 0 \\ 0 \\ 1 \end{bmatrix} E_0 = \begin{bmatrix} \sin\theta\sin\gamma \\ -\sin\theta\cos\gamma \\ \cos\theta \end{bmatrix} E_0 \qquad (4.65)$$

57

The average electric dipole moment induced $\bar{p}_{ee}$ by the excitation electric field $\overline{E}$ is:

$$\bar{p}_{ee} = \langle [T][T'][\alpha_{ee}]\overline{E} \rangle$$

thus

$$\bar{p}_{ee} = \langle [T] \begin{bmatrix} A_x \\ A_y \\ A_z \end{bmatrix} E_0 \rangle \tag{4.66}$$

where

$$
\begin{aligned}
A_x &= \cos\gamma \left(\alpha_{ee_{xx}} \sin\gamma \sin\theta - \alpha_{ee_{xy}} \cos\gamma \sin\theta + \alpha_{ee_{xz}} \cos\theta \right) \\
&+ \sin\gamma \left(\alpha_{ee_{yx}} \sin\gamma \sin\theta - \alpha_{ee_{yy}} \cos\gamma \sin\theta + \alpha_{ee_{yz}} \cos\theta \right) \tag{4.67} \\
A_y &= \cos\gamma \left(\alpha_{ee_{yx}} \sin\gamma \sin\theta - \alpha_{ee_{yy}} \cos\gamma \sin\theta + \alpha_{ee_{yz}} \cos\theta \right) \\
&- \sin\gamma \left(\alpha_{ee_{xx}} \sin\gamma \sin\theta - \alpha_{ee_{xy}} \cos\gamma \sin\theta + \alpha_{ee_{xz}} \cos\theta \right) \tag{4.68} \\
A_z &= \alpha_{ee_{zx}} \sin\gamma \sin\theta - \alpha_{ee_{zy}} \cos\gamma \sin\theta + \alpha_{ee_{zz}} \cos\theta \tag{4.69}
\end{aligned}
$$

Because T is independent of the rotation angle γ, we perform the averaging over spin first.

Since:

$$\frac{1}{2\pi} \int_0^{2\pi} d\gamma \cos^2\gamma = \frac{1}{2\pi} \int_0^{2\pi} d\gamma \sin^2\gamma = \frac{1}{2\pi}\frac{1}{2\pi} \int_0^{2\pi} d\gamma \cos\gamma \sin\gamma = 0$$

we get:

$$\bar{p}_{ee} = \langle [T] \begin{bmatrix} \frac{1}{2}\left(\alpha_{ee_{yz}} - \alpha_{ee_{xy}}\right) \sin\theta \\[2ex] \frac{1}{2}\left(\alpha_{ee_{xx}} + \alpha_{ee_{yy}}\right) \sin\theta \\[2ex] \alpha_{ee_{zz}} \cos\theta \end{bmatrix} E_0 \rangle$$

Thus

$$\bar{p}_{ee} = \langle \begin{bmatrix} C_x \\ C_y \\ C_z \end{bmatrix} E_0 \rangle \tag{4.70}$$

58

where

$$C_x = \frac{1}{2}\left(\alpha_{ee_{yz}} - \alpha_{ee_{xy}}\right)\sin\theta\cos\phi$$
$$- \frac{1}{2}\left(\alpha_{ee_{xx}} + \alpha_{ee_{yy}}\right)\sin\theta\cos\theta\sin\phi$$
$$+ \alpha_{ee_{zz}}\sin\theta\cos\theta\cos\phi \tag{4.71}$$
$$C_y = \frac{1}{2}\left(\alpha_{ee_{xy}} - \alpha_{ee_{yx}}\right)\sin\theta\sin\phi$$
$$- \frac{1}{2}\left(\alpha_{ee_{xx}} + \alpha_{ee_{yy}}\right)\sin\theta\cos\theta\cos\phi$$
$$+ \alpha_{ee_{zz}}\sin\theta\cos\theta\sin\phi \tag{4.72}$$
$$C_z = -\frac{1}{2}\left(\alpha_{ee_{xx}} + \alpha_{ee_{yy}}\right)\sin^2\theta + \alpha_{ee_{zz}}\cos^2\theta \tag{4.73}$$

We average now over orientation of helix:

Since:

$$\frac{1}{4\pi}\int_0^{2\pi} d\phi \int_0^{\pi} d\theta \sin\theta \sin^2\theta = \frac{1}{4\pi}\int_0^{2\pi} d\phi \int_0^{\pi} d\theta \sin\theta \cos^2\theta = \frac{1}{3}$$

while for all other terms the averaging gives 0, we finally get:

$$\overline{P}_{ee} = \begin{bmatrix} 0 \\ 0 \\ \alpha_{ee} \end{bmatrix} E_0 \tag{4.74}$$

Equation (4.74) shows that the averaged polarizability is scalar. We get similar result for any other fixed polarization of the excitation. Thus for a general excitation $\overline{E}$ the dipole moment is:

$$\overline{P}_{ee} = \begin{bmatrix} \alpha_{ee} & 0 & 0 \\ 0 & \alpha_{ee} & 0 \\ 0 & 0 & \alpha_{ee} \end{bmatrix} \overline{E} \tag{4.75}$$

where

$$\alpha_{ee} = \frac{\alpha_{ee_{xx}} + \alpha_{ee_{yy}} + \alpha_{ee_{xy}}}{3} \tag{4.76}$$

Similarly, the other averaged polarizabilities are:

$$\alpha_{em} = \frac{\alpha_{em_{xx}} + \alpha_{em_{yy}} + \alpha_{em_{zz}}}{3} \qquad (4.77)$$

$$\alpha_{me} = \frac{\alpha_{me_{xx}} + \alpha_{me_{yy}} + \alpha_{me_{zz}}}{3} \qquad (4.78)$$

$$\alpha_{mm} = \frac{\alpha_{mm_{xx}} + \alpha_{mm_{yy}} + \alpha_{mm_{zz}}}{3} \qquad (4.79)$$

Thus, for a given excitation, we have:

$$p_{e_j} \propto \begin{cases} \alpha_{ee_{jj}}, & \text{due to excitation} E_j \\ \alpha_{em_{jj}}, & \text{due to excitation} B_j \end{cases} \qquad (4.80)$$

$$p_{m_j} \propto \begin{cases} \alpha_{me_{jj}}, & \text{due to excitation} E_j \\ \alpha_{mm_{jj}}, & \text{due to excitation} B_j \end{cases} \qquad (4.81)$$

where j stands for x, y, or z

4.3   Calculation of the Effective EM Parameters

Once the polarizabilities are obtained the effective parameters of the composite medium can be calculated by applying the Lorenz-Lorentz form of the extension of the Maxwell-Garnett formula to the case of effective chiral media, presented in Section 3.3.

We test our model by comparing the theoretical predictions with the experimental results of [25] and [15] that use similar helix and medium parameters but different frequency region and experimental setup. In [25] a free-space experimental setup was used and the measurements were performed over a wide frequency range above the first helix resonance. In [15] the frequency range encompasses only the first resonance and the measurments are mainly performed using a waveguide experimental setup.

In both cases the effective EM parameters obtained numerically are used to calculate the impedance of the composite medium and in reflection and transmission calculations using the formulas of Sections 2.2, 2.3. Thus, using the obtained EM parameters we calculate also the difference $k_L - k_R$ whose real part is related to the rotation and the imaginary part is related to the dichroism as shown in Section 2.4.

60

Our results for the EM parameters are also used in (2.18) to calculate the reflection coefficient for a metal backed chiral slab of given thickness in comparison with the reflection of a metal backed slab of the host medium. The induced current and the backscattered fields for a single helix are also shown in every case since the frequency responce of the helix is expected to determine the behavior of the macroscopic medium EM parameters.

4.3.1 Wide Frequency Range

In this case we use as reference the measurements by Varadan et al. (1994) [25]. The helix and medium parameters used as input for our numerical modelling approximate the samples used in the experiment:

- Frequency: $8 - 40$ GHz

- Helix radius: 0.5842 mm

- Helix pitch: 0.5292 mm

- Wire radius 0.0787 mm

- Number of turns: 3

- Total length: 11.125 mm

- Wire Conductivity: 10^8 S/m

- Fractional volume of helices: $0.8\% - 3.2\%$

- Background relative permittivity: $2.6 + i0.5$

- Background relative permeability: $1 - i0.1$

With these helix and medium parameters the first $\lambda/2$ helix resonance is expected at around 8.3 GHz and higher order resonances at multiples of this frequency. The maximum absolute current and the backscattered fields for excitation $\overline{E}^i = \hat{x}e^{ik_0 y}$ are shown in Figure 4-4, where we can see a sharp resonance at about 25 GHz.

61

Maximum Helix Current

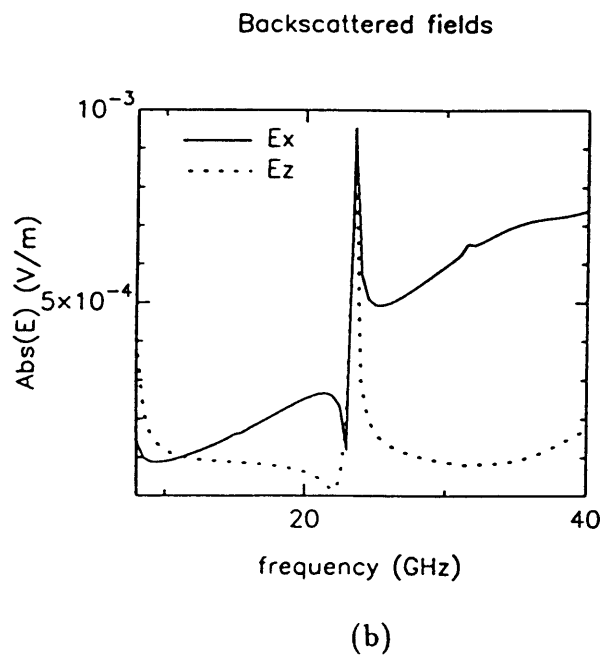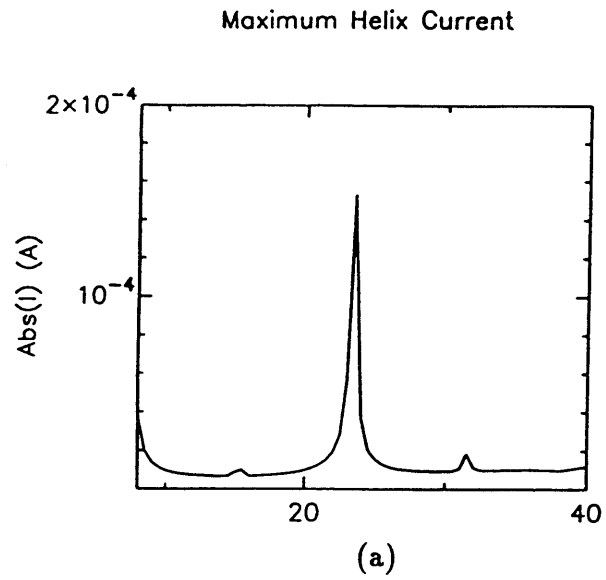
(a)

Backscattered fields

(b)

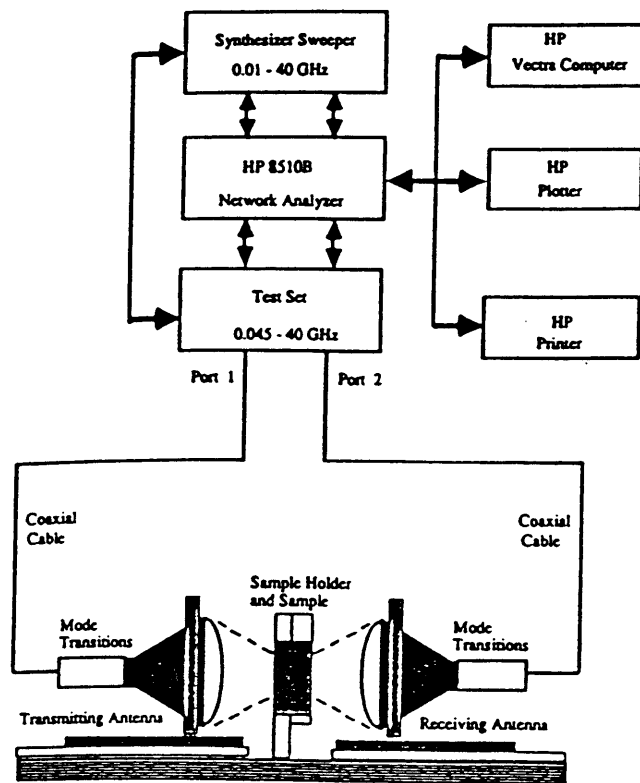Figure 4-4: Helix response (a) maximum current (b) backscattered fields

Figure 4-5: Free-space experimental setup used in measurements

63

A free-space setup consisting of a pair of spot-focusing horn antennas was used in the measurements (Figure 4-5). The antennas provide normal plane wave illumination on planar chiral samples of finite thickness. As previously discussed, the transmitted wave is elliptically polarized with its major axis rotated from the direction of linear polarization of the incident wave. Measuring the copolarized reflected wave and determining the ellipse of the transmitted wave with the measurement techniques described in Section 2.4, sufficient relations are obtained to solve for the three complex material properties. Thus the effective EM parameters were determined by inversion of transmission and reflection measurements while ambiguities encountered in the inversion algorithm were removed with a new procedure using time domain response.

The samples used in these measurements are prepared by embedding a large number of either left-handed or right-handed miniature metal helices with the parameters given above, in an epoxy host material. The matrix material, Eccogel, is homogeneous, isotropic and achiral with $\epsilon \simeq 2.6 + i0.5$ and $\mu \simeq 1 - i0.1$ at 25 GHz. The samples have metal volume concentration varying from 0.8% (37 springs/cm^3) to 3.2% (147 springs/cm^3). Due to the large excluded volume within each helix, the closest packing fraction for helices is very low, of the order of 6% − 7%, hence the concentrations used here are high. The sample consists of two layers one layer contains a random dispersion of helices in Eccogel and the other contains only Eccogel and is needed to ensure the random orientation of the dispersed springs. The EM properties of a pure Eccogel sample were determined so that the EM parameters of the chiral composite without the effect of the Eccogel layer could be determined by using a two layer inversion method. Details on the construction of the samples and the experimental setup have been desrcribed by Guire et al. (1990) [21].

Our theoretical predictions in comparison with the experimental results are shown in Figures 4-6 - 4-10. In addition, we have calculated the reflection coefficient for normal incidence on a chiral slab of thickness 2.14 cm, over a perfect conductor (Figure 4-11)
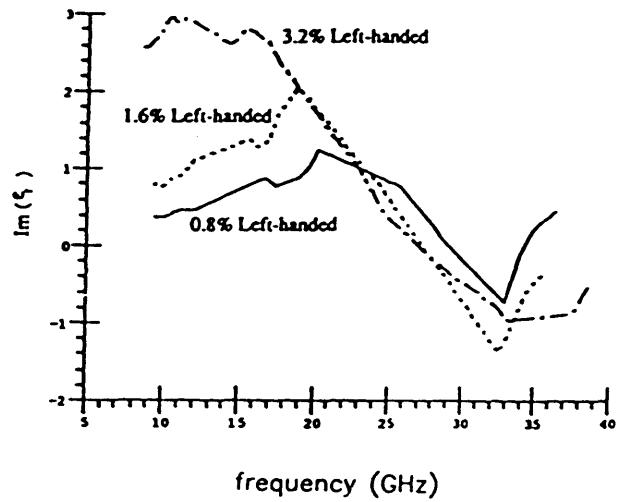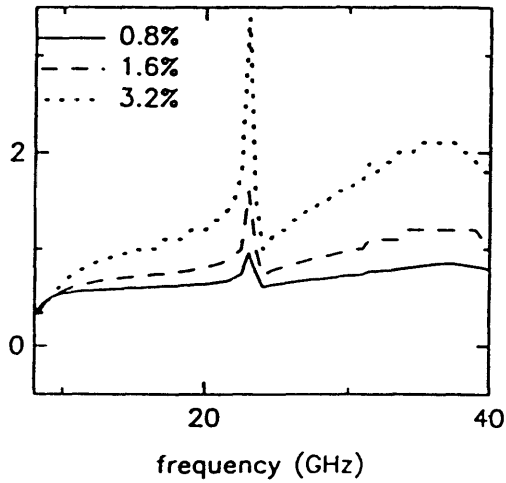
As can be seen in Figures 4-6 and 4-7 there is a rapid variation of ϵ and μ with frequency around the resonance frequency at 25 GHz, which in the experimental
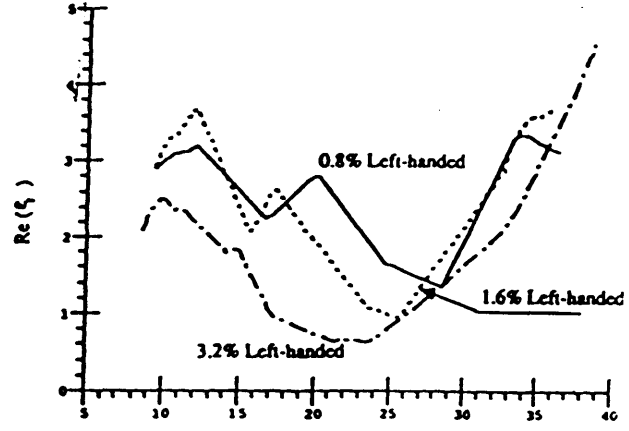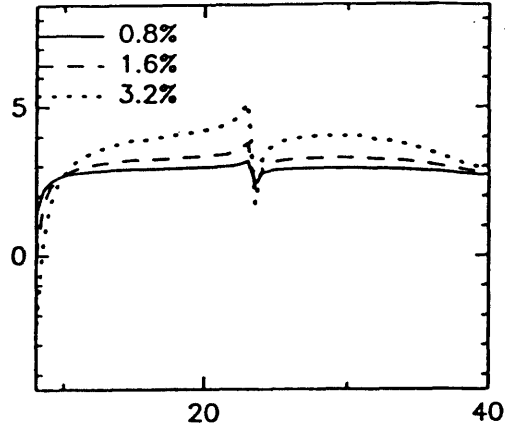
Figure 4-6: Relative permittivity: (a)numerical results (b)experimental results

Relative Permeability (Real Part)

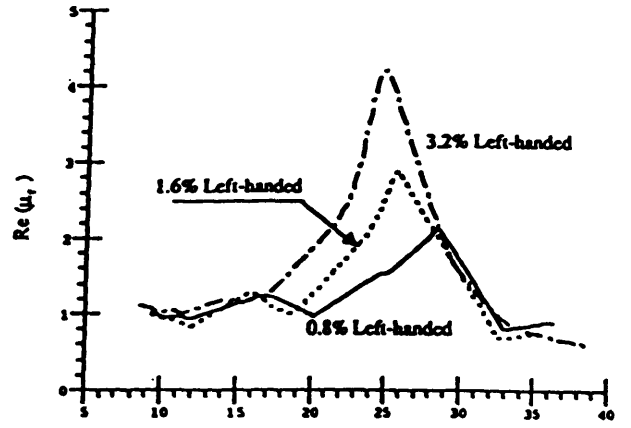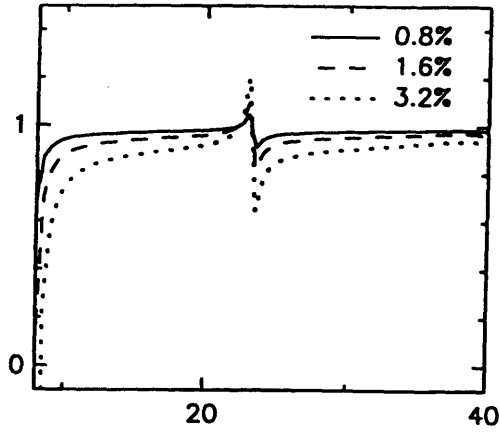## Relative Permeability (Imaginary Part)

frequency (GHz)

(a)

frequency (GHz)
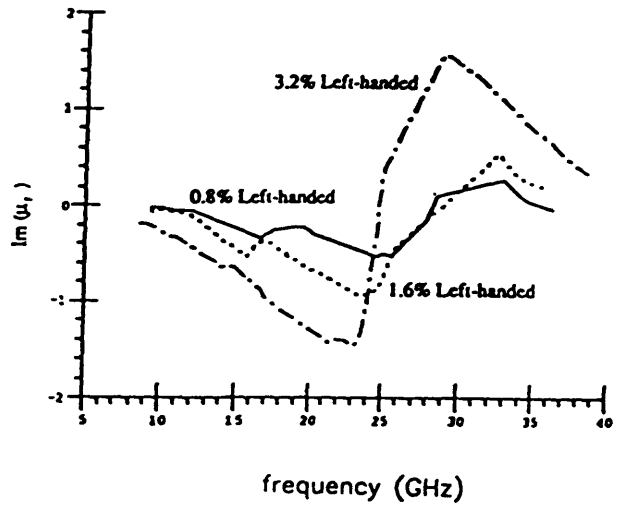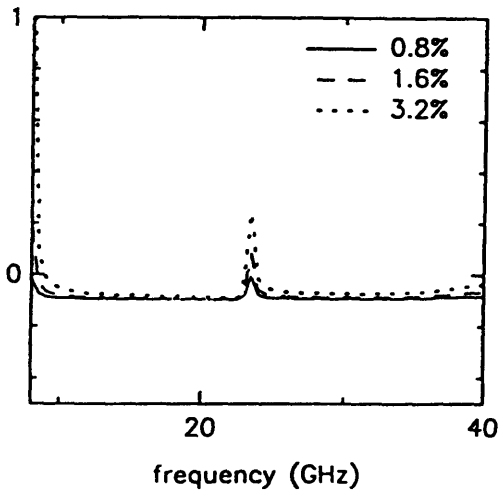
(b)

Figure 4-7: Relative permeability: (a)numerical results (b)experimental results

Chirality (Real Part)
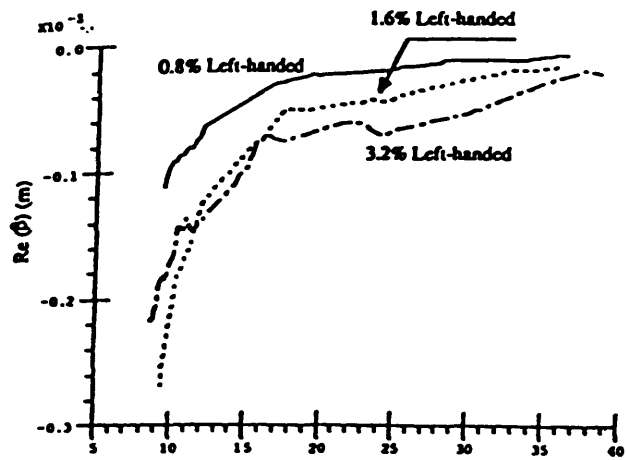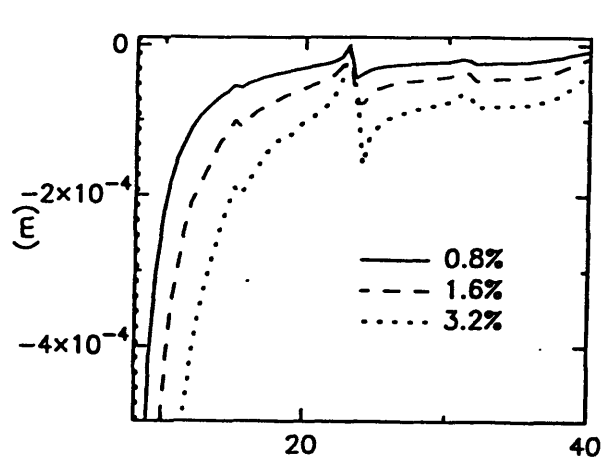
Chirality (Imaginary Part)
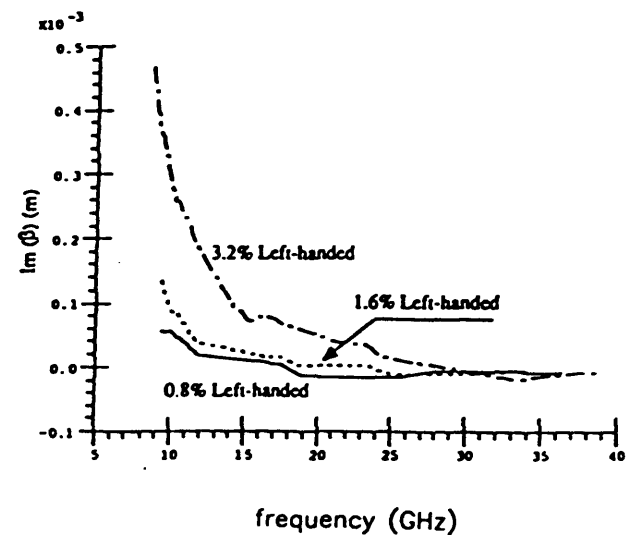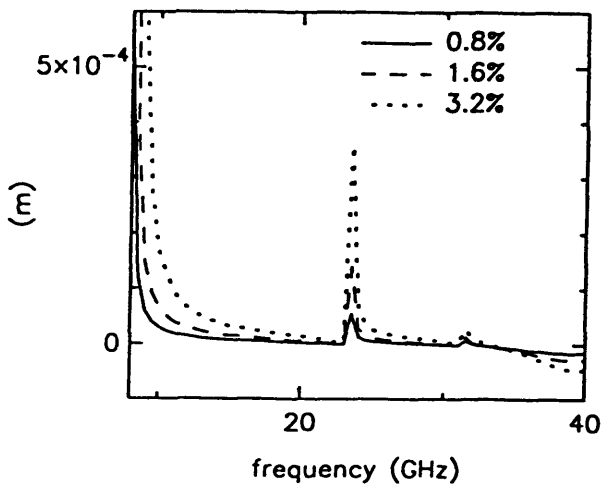
(a)

(b)

Figure 4-8: Chirality: (a)numerical results (b)experimental results

Impedance(Real Part)
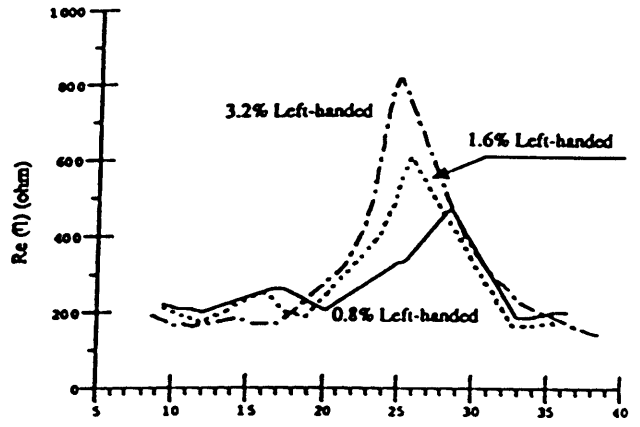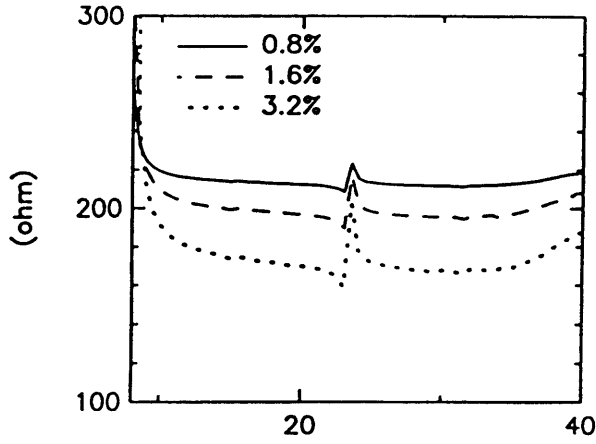
Impedance(Imaginary Part)
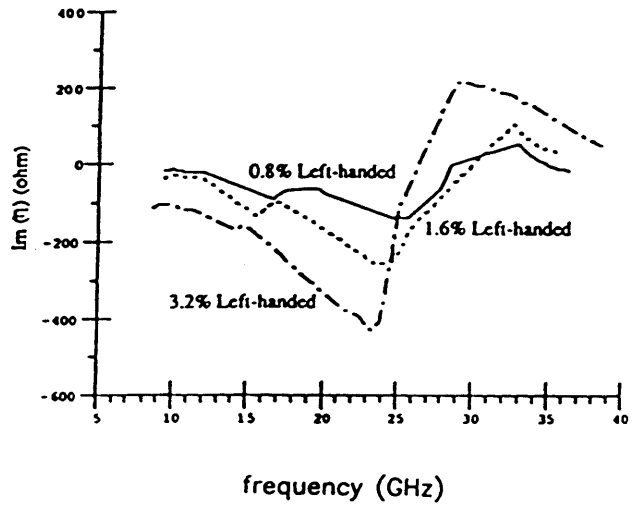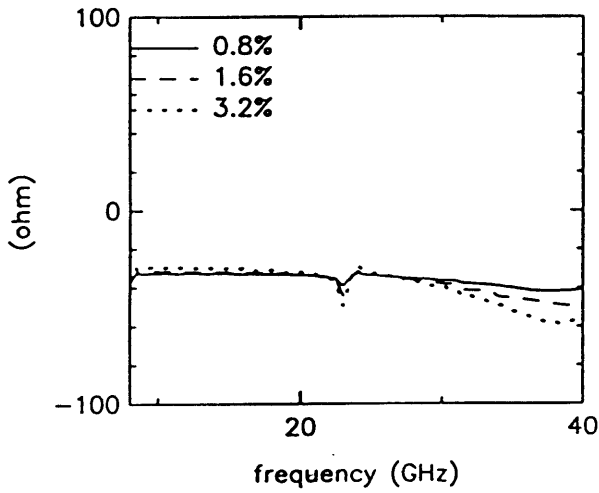
(a)

(b)

Figure 4-9: Medium impedance: (a)numerical results (b)experimental results

68

Difference of Wavenumbers(Real Part)
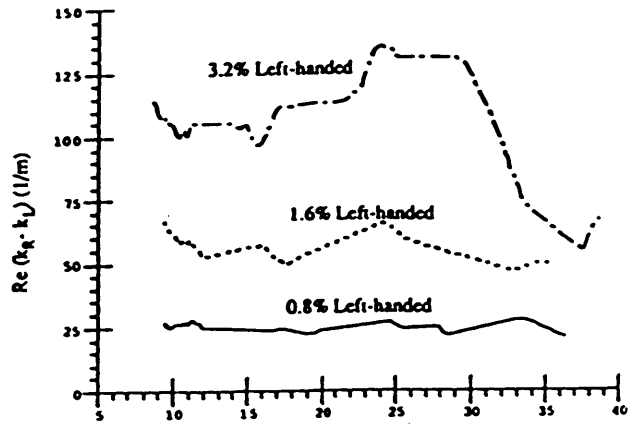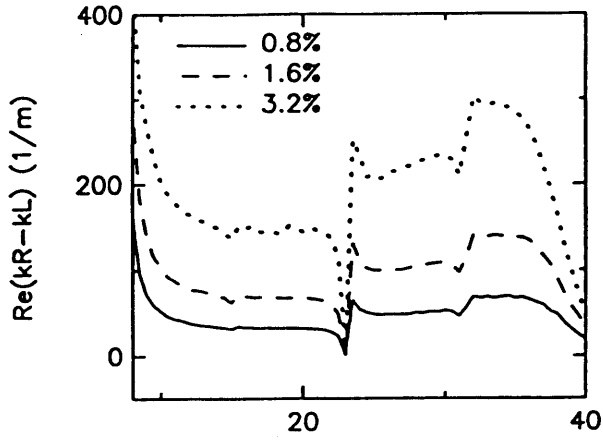
Difference of Wavenumbers(Imaginary Part)
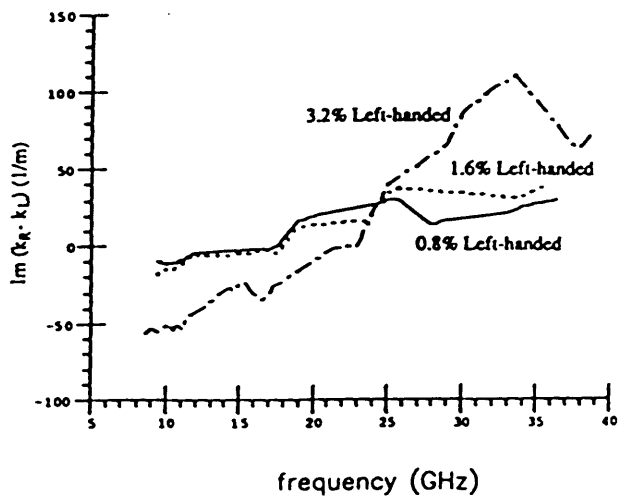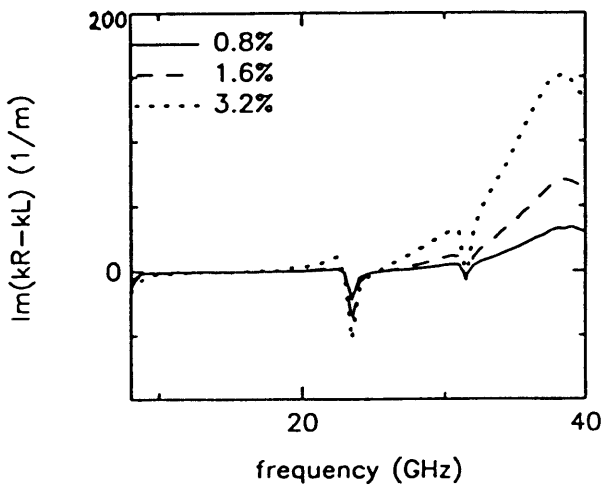
(a)

(b)

Figure 4-10: Difference of wavenumbers for LCP and RCP: (a)numerical results (b)experimental results

Power Reflection Coefficient

(0.8%)

(1.6%)

(3.2%)
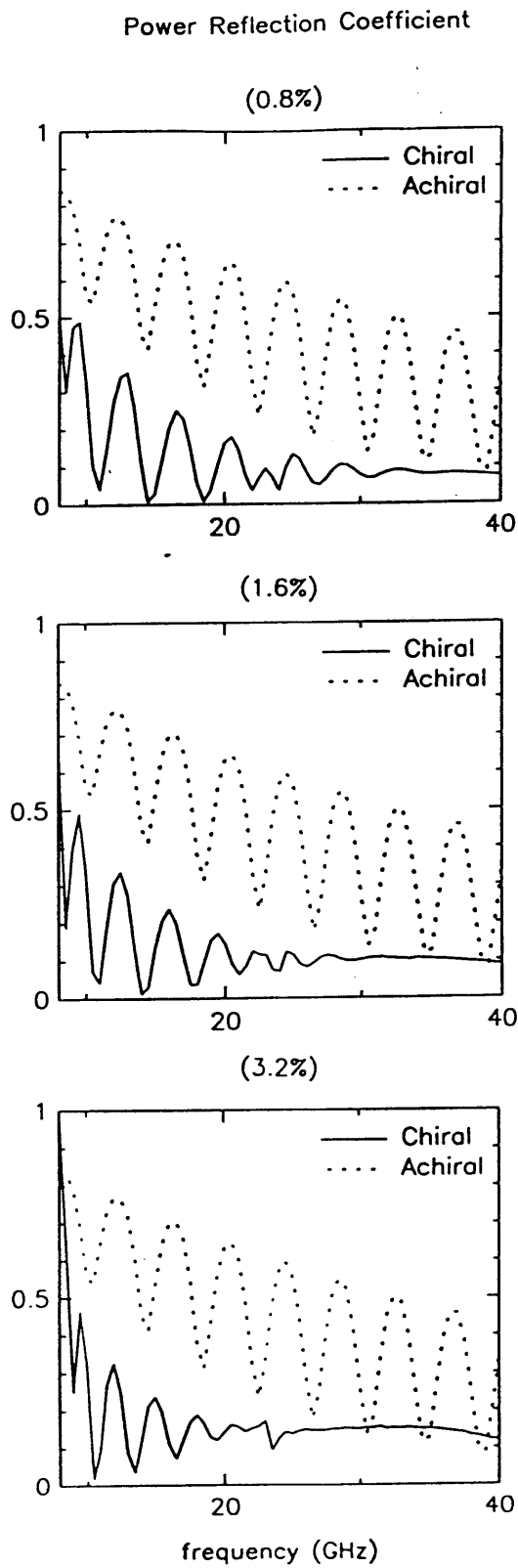
frequency (GHz)

Figure 4-11: Reflection coefficients for metal backed slab of thickness 2 cm for the composite and the host material respectively

results extends in a wide frequency range while in the numerical results there is a sharp resonance at 25 GHz but of much smaller magnitude in most cases. The same effects can be observed in Figure 4-9 for the impedance since this depends on the effective permittivity and permeability. Thus the theoretically predicted resonace is again much narrower around 25 GHz and much weaker than the measured.

On the other hand, the behavior of chirality with frequency is relatively well predicted as can be seen in Figure 4-8 and the theoretical curves are close to the experimental curves, but with a sharp resonance at 25 GHz which is absent from the measurements. Similarly, the qualitative behavior of the difference $k_R - k_L$ which is related to the effects of optical activity and hence to chirality, is not far off from the experimental results. In the later, however the resonance does not appear as sharp.

In Figure 4-11 the reflection coefficient for a metal backed chiral slab is compared to that of the host medium. Although the results are not very different we can see that the introduction of chirality has an effect in reducing the reflected power.

4.3.2 Narrow Frequency Range

In this case we use as reference the measurements by Hollinger et al. [15] . The helix and medium parameters used as input for our numerical modelling approximate the samples used in the experiment:

- Frequency: $5 - 10$ GHz

- Helix radius: 0.625 mm

- Helix pitch: 0.667 mm

- Wire radius 0.0762 mm

- Number of turns: 3

- Total length: 11.95 mm

- Wire Conductivity: 10^8 S/m

- Fractional volume of helices: $0.8\% - 1.6\%$

- Background relative permittivity: $2.95 + i0.07$

- Background relative permeability: 1

With these helix and medium parameters the first $\lambda/2$ helix resonance is expected at around 7.3 GHz. Higher order resonances occur at multiples of this frequency and are not included in this frequency range. The maximum absolute current and the backscattered fields for excitation $\overline{E}^i = \hat{x} e^{ik_0 y}$ are shown in Figure 4-12.

A waveguide setup was mainly used in the measurements, where the chiral samples were placed in a circular waveguide. The waveguide propagates the TE_{10} mode and near its center this mode approximates a plane wave incidence on the chiral sample, while multiple reflections and errors in measurement have been sufficiently reduced. The polarization ellipse is determined as described in Section 2.4 only now instead of receiving antenna we have a waveguide. The results obtained with the waveguide
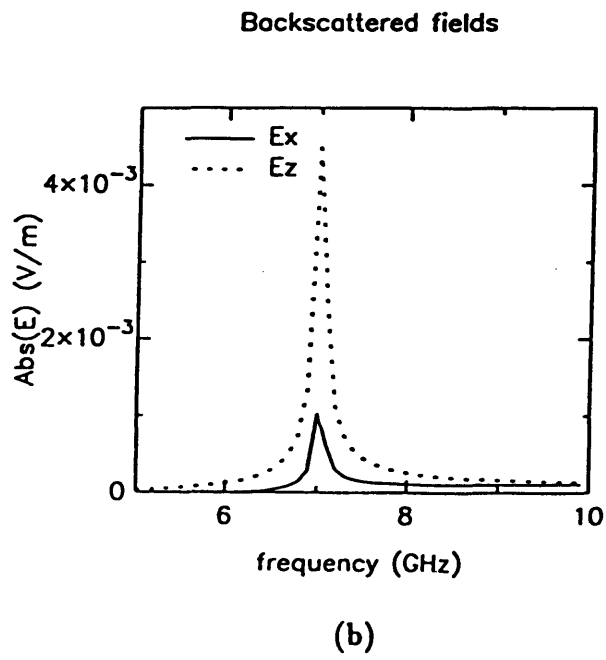
Maximum Helix Current

(a)

Backscattered fields

(b)
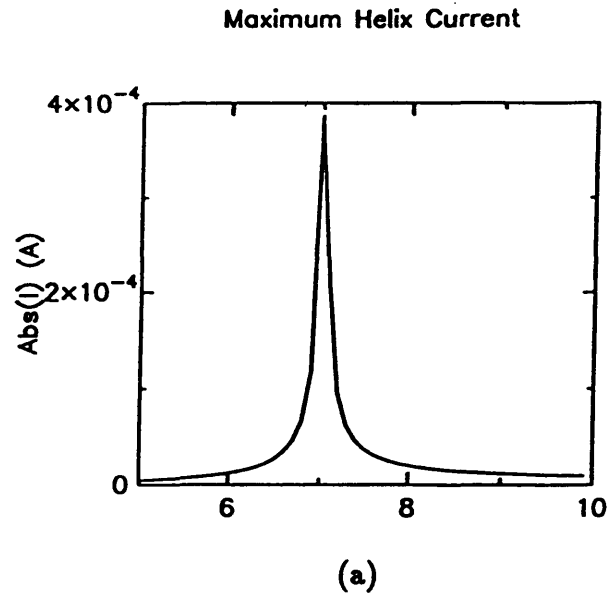
Figure 4-12: Helix response (a) maximum current (b) backscattered fields

73
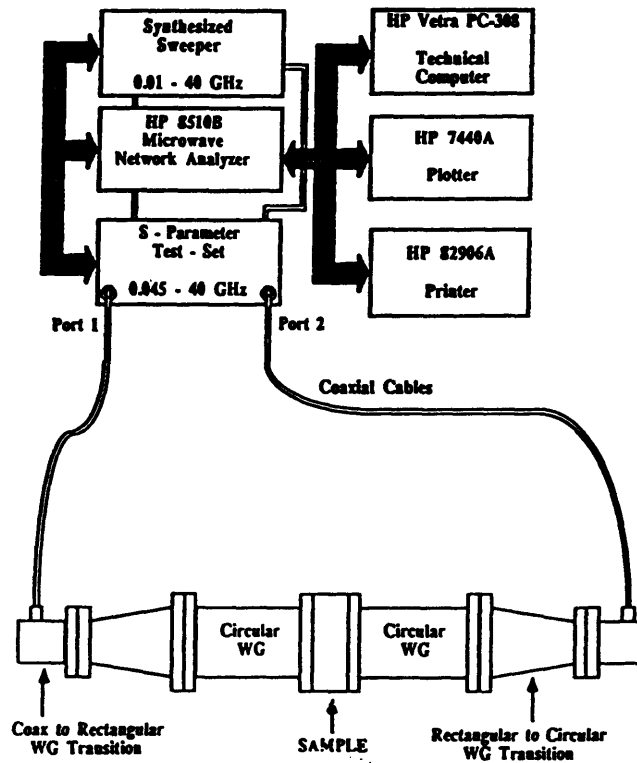
Figure 4-13: Waveguide experimental setup used in measurements

setup were also compared and found remarkably similar to results obtained using the free-space setup previously described.

The composite samples here were made of copper helices with the dimensions given above, embedded in silicon rubber and had thickness 2.14 cm for the waveguide measurements and 0.625 cm for the free-space measureements. More details on the sample preparation the experimental stup and the measurements are given in [15].

The measurements are focussed on the effects optical activity (rotatory dispersion and circular dichroism) and were not inverted to obtain the effective parameters. In our numerical modelling, however, we calculate the effective EM parameters of the medium and the results are used to obtain the reflection and transmission characteristics. The experimental results are shown here rather as reference for the frequency response of our model around the first resonance. Our predictions for the EM parameters and the impedance are shown in Figures 4-14 and 4-15 and the results are used to calculate the reflection coefficients as before (Figure 4-16). The difference of wave numbers and the axial ratio are shown for both concentrations in figure 4-17 and the experimental results for the rotation and the axial ratio are given in figure 4-18.

With the first $\lambda/2$ helix resonance included in this frequency range, our results for the effective EM parameters (Figures 4-14 and 4-15) exhibit a very sharp and strong resonace at around 7 GHz. The calculated values are much higher than in other published modelling works such as [1],[28],[17] and . the medium parameters have a large negative real part just before the resonance frequency. This effect has an impact at the calculated reflection coefficients for a metal backed slab (figure 4-16), thus although there is a trend to reduce the reflected power there is an anomaly around 7 GHz and the medium becomes active. Thus, our model gives non physical results around the first resonance. This can be attributed to the breakdown of the Maxwell-Garnett mixing formula near the resonance.

In our results for the difference $k_L - k_R$ we can see that the change of sign of the real part, that occurs at the resonace frequency corresponds to a change of sign in the experimental results for the rotation angle. The calculated axial ratio which

Relative Permittivity (Real Part)

Relative Permittivity (Imaginary Part)

Relative Permeability (Real Part)

frequency (GHz)

Relative Permeability (Imaginary Part)

frequency (GHz)
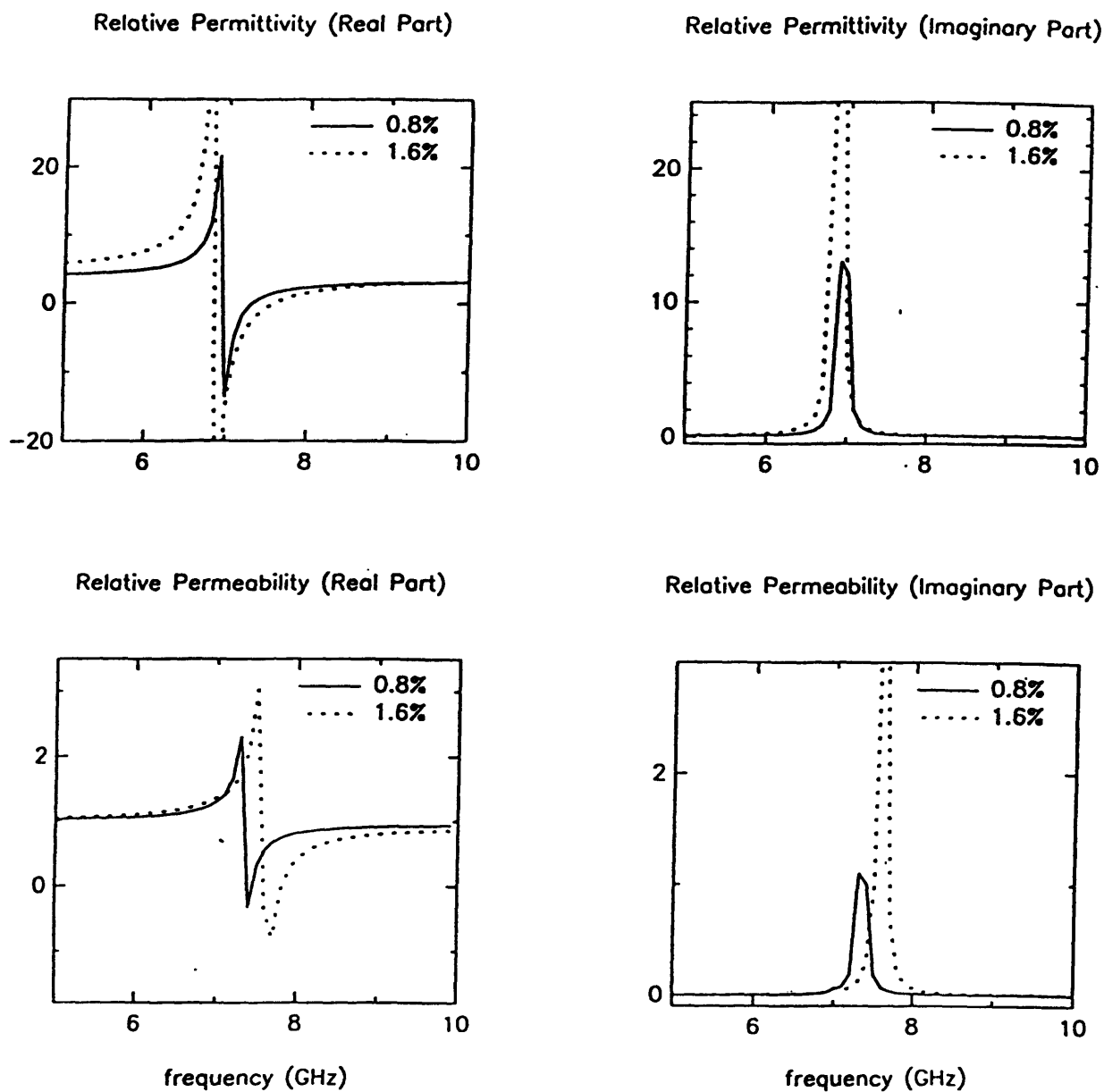
Figure 4-14: Numerical results for relative permittivity and permeability

Chirality (Real Part)

Chirality (Imaginary Part)

Impedance (Real Part)

Impedance (Imaginary Part)
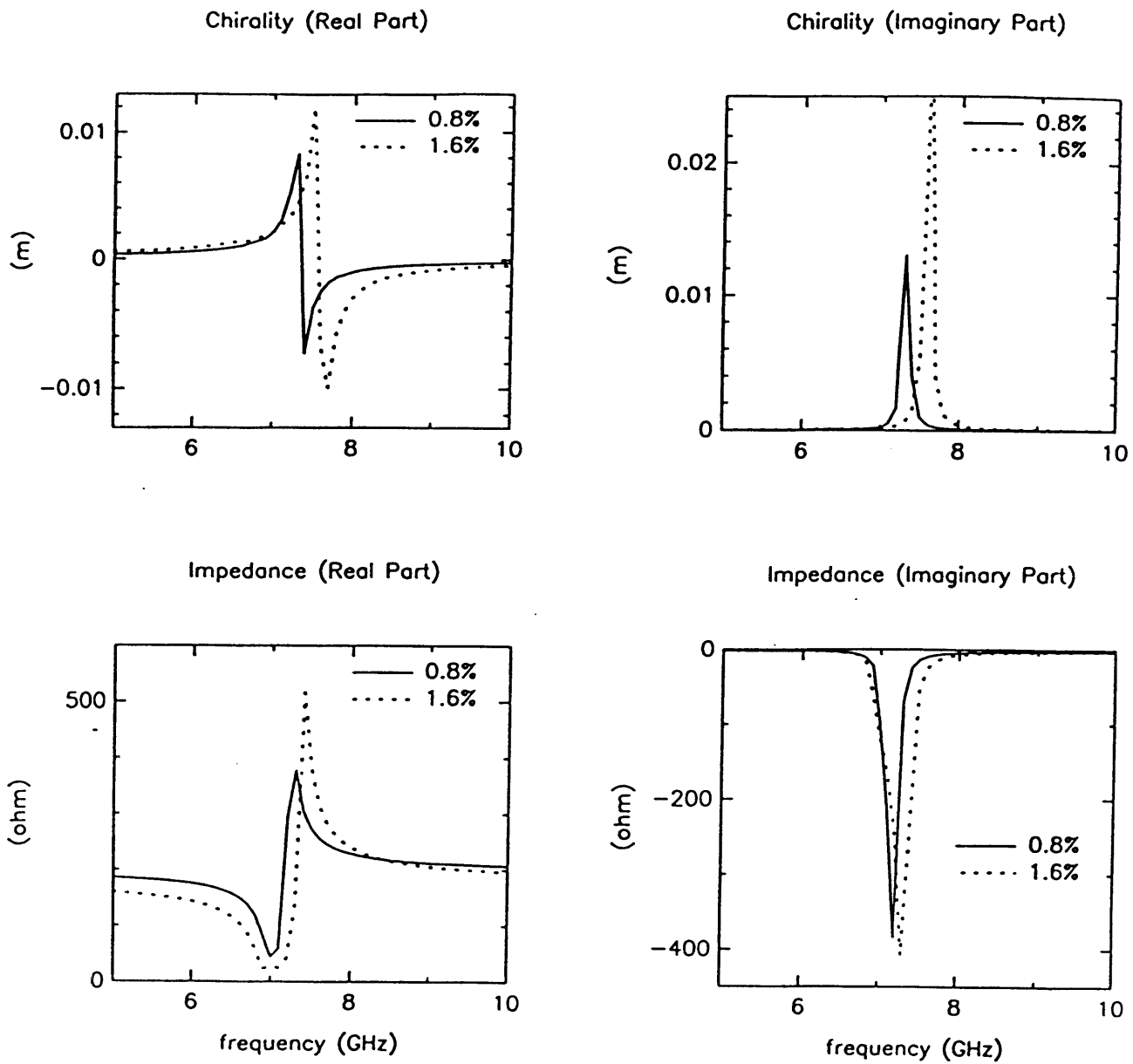
Figure 4-15: Numerical results for chirality and impedance

Power Reflection Coefficient

(0.8%)

(1.6%)

frequency (GHz)
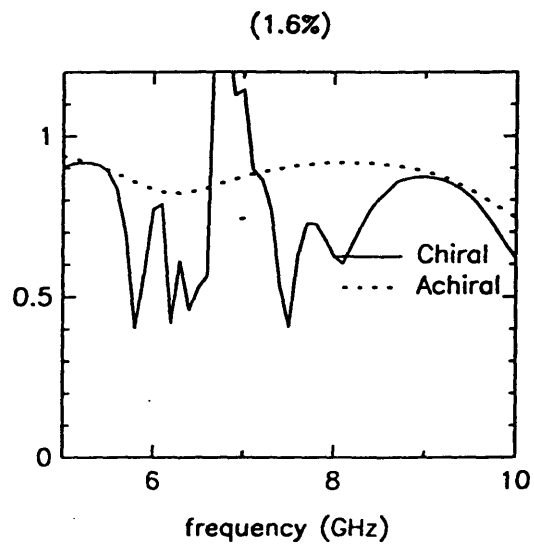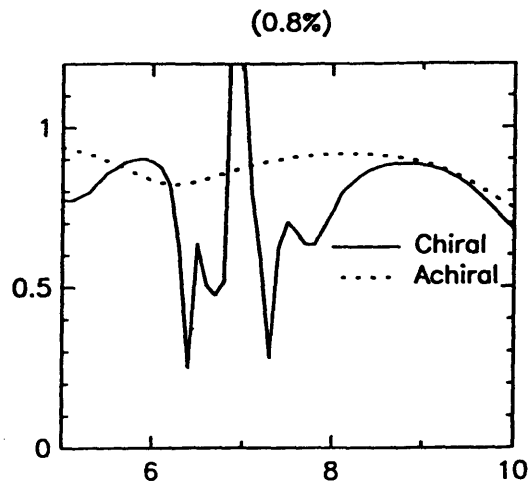
Figure 4-16: Reflection coefficients for metal backed slab of thickness 2.14 cm for the composite and the host material respectively
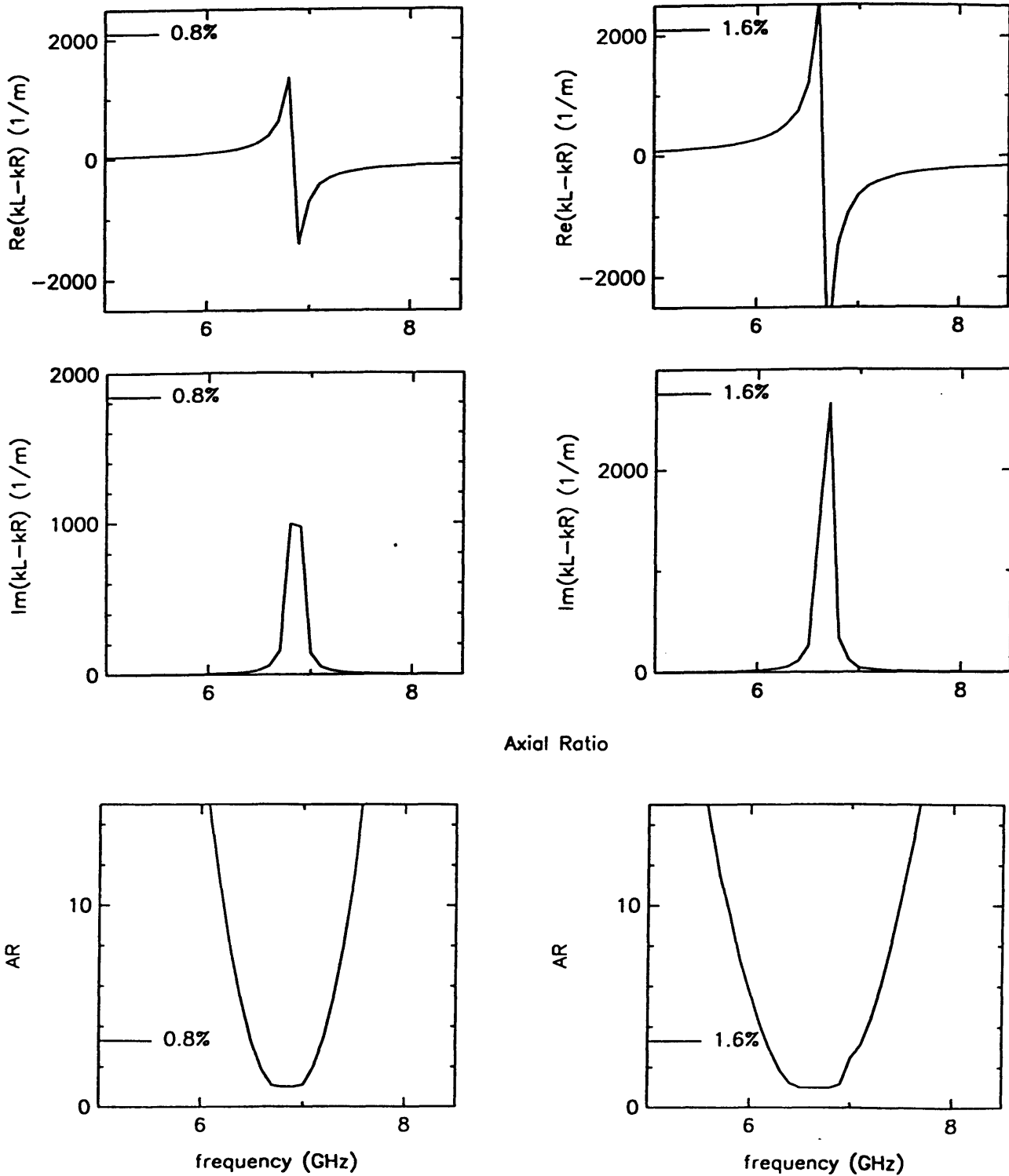
Figure 4-17: Numerical results for difference of wavenumbers for LCP and RCP and axial ratio
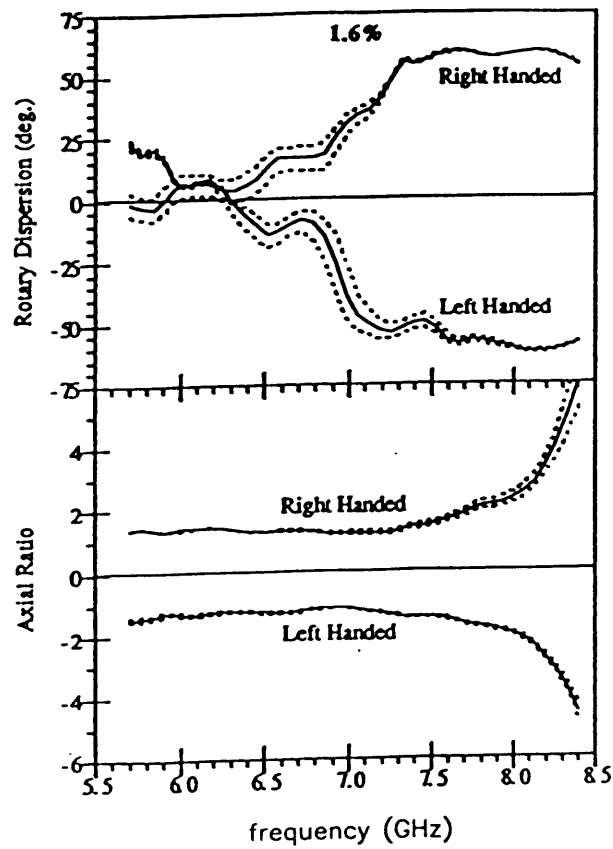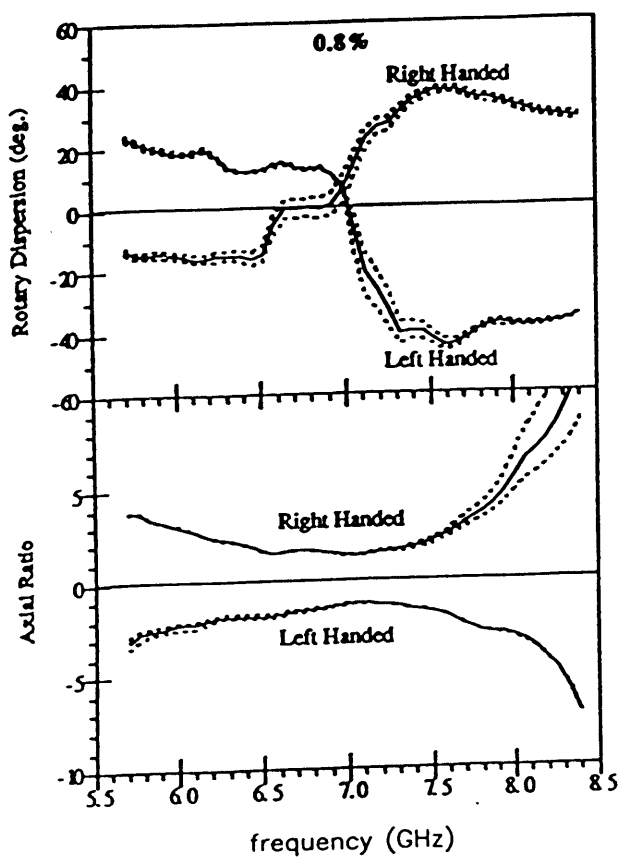
Figure 4-18: Experimental results for rotatory dispersion and axial ratio

depends on the imaginary part of $k_L - k_R$, agrees qualitatively with the measurements although the variation with frequency is more rapid and much narrower. In both cases the absolute value of the axial ratio is 1 around the resonance.

4.3.3 Sensitivity Study

It is interesting to see how the predicted EM properties of a helix loaded composite vary with the helix parameters. We focus on the variations with helix conductivity and pitch-to-radius ratio and the calculations are performed in the case of very low inclusion and at frequency far below the first $\lambda/2$ resonance. Therefore, we expect the assumptions of the Maxwell-Garnett mixing law to be valid.

The following input parameters were chosen as the defaults in the sensitivity study.

- Total length of wire: 1.56 mm

- Wire radius: 3.8μm

- Pitch/Radius ratio: 2

- Number of turns: 1

- Wire Conductivity: $1 - 10^8$ S/m, power of 10

- Frequency $1 - 10$ GHz

- Fractional volume of helices: 0.08%

- Background relative permittivity: 2.05

- Background relative permeability: 1

With these helix and medium parameters the first $\lambda/2$ helix resonance is expected at around 67 GHz.

A number of calculations were performed varying one of these parameters while the rest remained constant. The variation with frequency was found to be almost negligible, as the helices were always much smaller than a wavelength in this frequency

Relative Permittivity (Real Part)

Relative Permittivity (Imaginary Part)

Relative Permeability (Real Part)

Relative Permeability (Imaginary Part)

Chirality (Real Part)

Chirality (Imaginary Part)

log(conductivity)
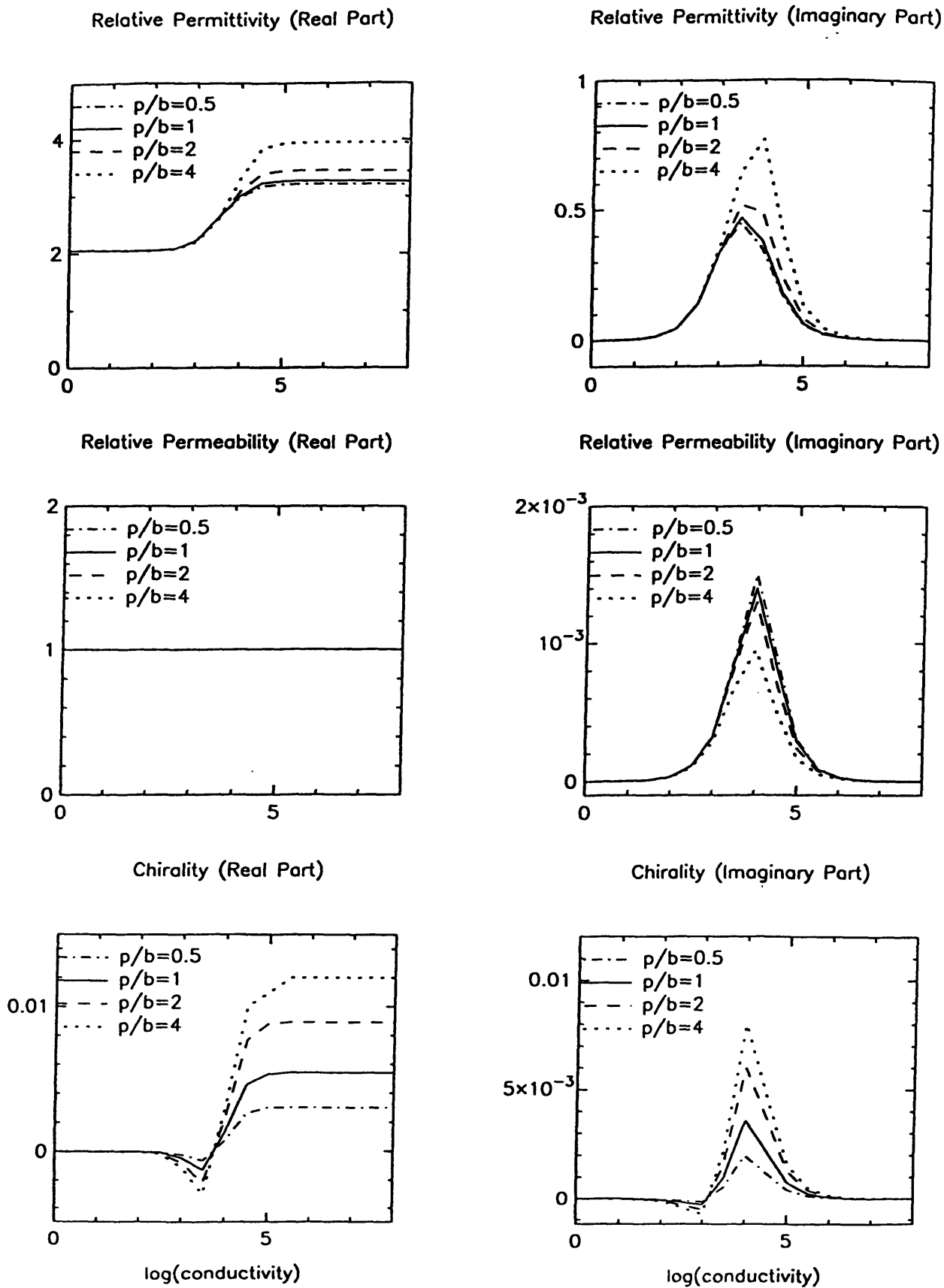
log(conductivity)

Figure 4-19: Effective EM parameters calculated at 10 GHz varying conductivity and pitch-to-radius ratio
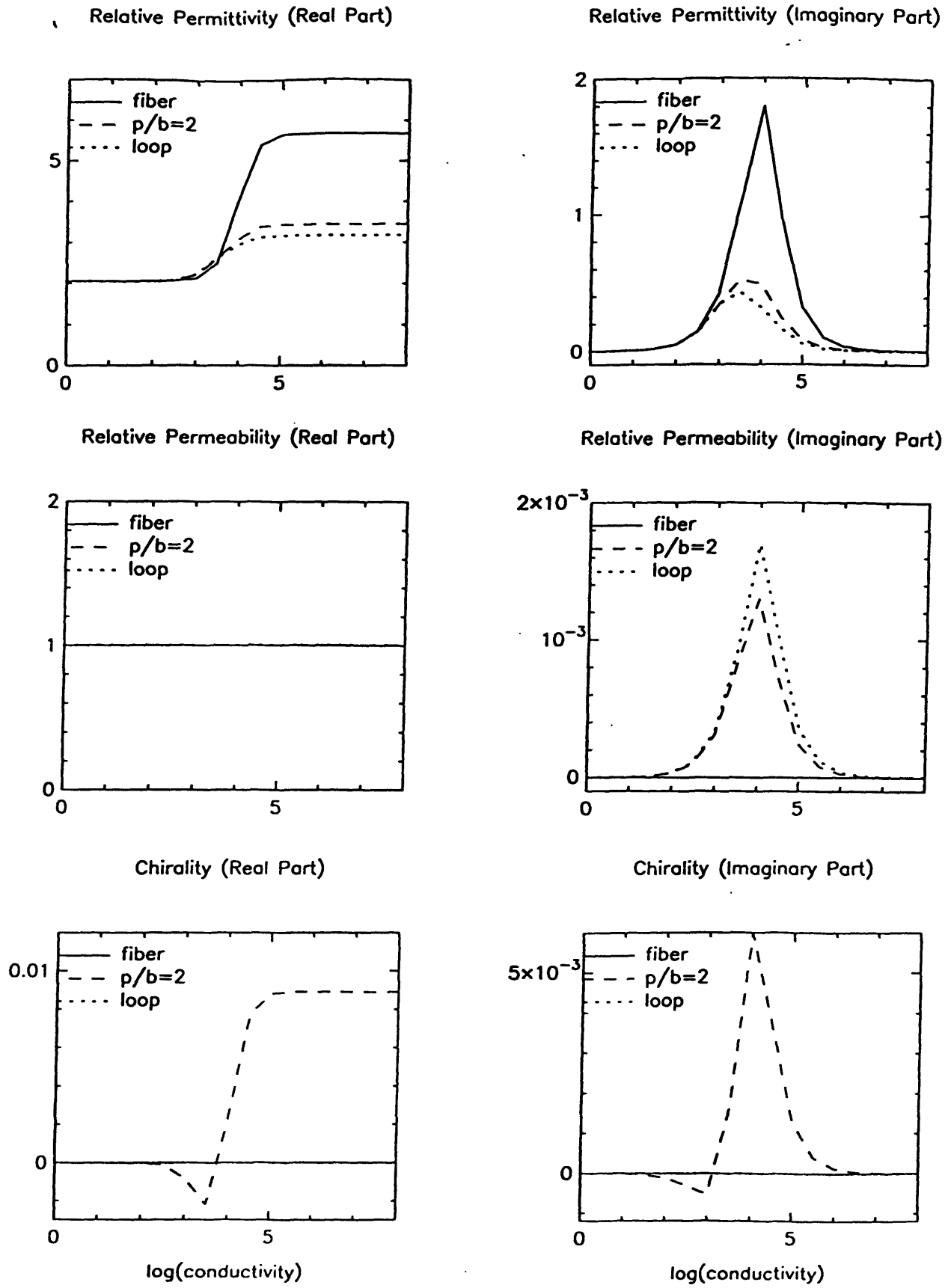
Figure 4-20: Effective EM parameters calculated at 10 GHz varying conductivity and pitch-to-radius ratio

range, except for the expected resonant behavior in the imaginary part of the electro-magnetic parameters for wires with intermediate conductivities. This resonance was found both in the permittivity and the chirality; however, the relative permeability showed almost no change from the background value of unity. For a fixed wire length, a pitch/radius ratio between 4 and 5 was found to give the largest values of chirality (as can be seen also in Figure 4-19), as concluded also in [18],[23] and one turn was found to be optimal. Longer wire lengths showed correspondingly larger effects, so that the problem seems to be driven primarily by the electric dipole behavior of the included helices.

The variation with conductivity at $f = 10$ GHz is shown in Figures 4-19 and 4-20. In the latter we verify the fact that long fibers and loops do not introduce chirality in the medium since, in that case, the inclusions are not handed. And while the inclusion of long fibers affects only the permittivity, the inclusion of loops affects both the permittivity and the imaginary part of permeability where the largest effect is observed.

Except the real part of the permeability where there is no effect, in the interme-diate conductivities (around $10^4 \mho$) the real parts vary rapidly from above the host medium values and remain stable until the case of peerfect conductor. The imaginary parts exhibit a "resonance" at intermediate conductivities.

The reflection coefficients for a metal backed chiral slab were again calculated using the obtained medium parameters. Although values for chirality were obtained by including helices in the medium, the reflection coefficients showed little effect and the permitivitty seems to be the principal component driving the problem in the low frequency and low fractional volume limit.

4.4 Conclusions

As we have seen above, there is a poor match of the predictions of our model, com-pared to published data. The only point of agreement is the resonance frequency and the qualitative behavior of the effective electromagnetic parameters with fre-

quency. The expected $\lambda/2$ resonace frequencies were obtained with small errors, and the calculated effective parameters were found to be strongly dependent on frequency near resonance. The resulting effective electromagnetic parameters show a resonant frequency dependence similar to that of the helix current. The current in the wire helices shows a resonant maximum which occurs when the wire length is near half a wavelength, regardless of how tightly wound the helix is.

Chirality as well as permittivity and permeability increase in amplitude and vary rapidly near the first resonance and the real part changes sign. The effect is greater on the permittivity than the permeability. Helix resonance also causes the polarization rotation and the absorption to vary rapidly with frequency.

Although the qualitative behavior of the EM parameters is predicted, the resonances found are much sharper than in the references we used, especially the first $\lambda/2$ resonance, and the calculated maximum values differ considerably from the measured data, being much higher around the first resonance and usually lower around higher order resonances.

The discrepancies with the published data are due to the breakdown of the Maxwell-Garnett mixing law whose validity is limited to frequencies much lower than the resonance and to low inclusions, while the cases examined were over a wide range of frequency and helix concentration. Also the thin wire approximation used in our approach is valid for wire diameter $< 0.01\lambda$ so our results become less accurate at higher frequencies.

The effects on reducing the reflection from a metal backed slab are limited to narrow frequency bands and it is believed that, in order to achieve broader optically active frequency ranges, different sizes of helices should be included in the sample[1].

The mixing law applied in the modelling of helix loaded composites is limited to the case of low inclusion and low frequencies, and consequently to low chirality of the medium, while it appears that in order to obtain considerable chirality effects higher concentrations and larger inclusions are needed. Extensions beyond these limitations will require a new method applicable to such configurations. An alternate approach to this problem, investigated in the next chapter, could be based upon a

numerical solution of the exact integral equation for a composite medium made up of periodically spaced helices. Once the currents induced on the helices are obtained using the method of moments, reflection and transmission calculations for a slab of given thickness could be inverted to give the effective EM parameters.

Chapter 5

Periodic Helix Structures

5.1 Introduction

Most of the methods of analysis for artificial media, including the Maxwell-Garnett mixing law, are based upon static or quasi-static approximations and often include only the lower order multipoles. For this reason, as has been previously discussed, such methods are limited to electrically small scatterers and low concentrations.

Another general approach can be a full wave analysis based upon a MoM solution of an exact integral equation for the equivalent currents on the scatterers [10]. The MoM accounts for mutual coupling between the scatterers and is applicable to artificial media comprising scatterers of essentially arbitrary size, shape and material composition, and is capable of determining the dispersion characteristics of the artificial medium. The scatterers are assumed to be identical and arranged in an infinite periodic lattice. This simplification allows the scattering problem to be reduced to that of a single scatterer. Using the periodic method of moments (PMM), the unknowns of the equation can be limited to those of the center element. Thus, due to the periodicity of the medium and of the plane incident field, the current on each element is identical except a phase and amplitude shift, corresponding to the amplitude and phase of the plane wave at the reference point of each element.

The periodic artificial medium can be modeled as a triple infinite periodic array of identical scattering elements in some homogeneous isotropic background with per-

mittivity ϵ_0 and permeability μ_0 and wavenumber $k_0 = \omega\sqrt{\epsilon_0\mu_0}$. The basic problem is to determine whether or not the periodic medium appears as an artificial medium, and if so, by determining whether a plane wave is an eigenfunction of the periodic medium, and if so, what is the eigenvalue or complex phase constant of that plane wave [10]. In this case, an eigenfunction is a source-free solution of Maxwell's equation that satisfies all the boundary conditions. To find the eigenfunctions, a plane wave of a known frequency ω is assumed to be propagating in the periodic medium in a known direction but with unknown polarization and phase constant k_e.

The periodic array of scatterers is replaced by the host medium and by equivalent currents, which due to the priodicity of the medium and of the plane wave field, are identical on each element, except for an amplitude and phase shift corresponding to the amplitude and phase of the plane wave at the reference point of each element.

The next step is to formulate an integral equation for the equivalent eigenfunction current J. The current is expanded in a set of basis functions. Applying the PMM the unknown expansion coefficients are the solutions of a matrix equation of the form:

$$[Z(k_e)]\bar{I} = 0 \qquad (5.1)$$

where $[Z(k_e)]$ is the impedance matrix and $\bar{I}$ is the vector of the unknown expansion coeffients of the current. As can be seen by (5.1) the elements of the impedance matrix depend on the unknown phase constant k_e. Equation (5.1) will have a non-trivial solution if the determinant of the impedance matrix is zero:

$$|Z(k_e)| = 0 \qquad (5.2)$$

Equation (5.2) must be solved for the eigenvalues k_e which yield non-trivial solutions of (5.1). If a solution of the characteristic equation (5.2) exists, then the periodic medium can be viewed as an artificial medium. The induced currents that correspond to the eigenvalue k_e yield the eigenfunction fields and the the characteristic impedance η_e of the medium can be found as the ratio of the electric and magnetic eigenfunction fields tangential to the assumed direction of propagation with effective EM parameters

that can be found through the eigenfunction fields and the characteristic impedance.

In a simplified approach to the analysis of a periodic artificial medium, we assume propagation with the background wavenumber in a known direction and polarization. The currents that are induced on the scatterers could then yield the scattered fields due to given excitation. Hence, reflection and transmission calculations for given thickness and given incident field could give by inversion the effective parameters of the medium. The formulation for this approach is presented for the case of a superposition of a finite number of two-dimensional periodic arrays made up of aligned helices.

5.2   General Formulation

Consider a planar periodic structure in the $x - y$ plane at $z = z_0$. The periodicity is along the x and y directions, thus we can divide the plane into similar unit cells with the center cell at the origin. The x and y distances between adjucent cells are the periodicities d_x and d_y, respectively.

Any of the unit cells is specified by the indices (m, n) that determine the x and y coordinates of the reference point of the cell. The relevant position vector is then:

$$\bar{r}_{mn} = md_x\hat{x} + nd_y\hat{y} \tag{5.3}$$

and any source point in the periodic structure is described by the position vector:

$$\bar{r}'_{mn} = \bar{r}' + \bar{r}_{mn} \tag{5.4}$$

where $\bar{r}'$ is the source point on the center element.

Using the equivalence principle we replace the periodic structure by an equivalent volume or surface current $\bar{J}_s$ which due to the periodicity of the medium and its fields satisfies the condition:

$$\bar{J}_s(\bar{r} + \bar{r}_{mn}) = \bar{J}_s(\bar{r})e^{i\bar{k}_t \cdot \bar{r}_{mn}} \tag{5.5}$$

where the propagation vector is:

$$\overline{k} = \overline{k}_t + k_z \hat{z} \tag{5.6}$$

We can therefore define a scalar planar-periodic Green's function $g_p(\overline{r}, \overline{r}')$ that includes the phase shift between the adjucent elements :

$$g_p = \sum_{m,n} g(\overline{r}, \overline{r}' + \overline{r}_{mn}) e^{i\overline{k}_t \cdot \overline{r}_{mn}} \tag{5.7}$$

where $g(\overline{r}) = e^{ikr}/4\pi r$ is the scalar Green's function and:

$$\sum_{m,n} = \sum_{m=-\infty}^{+\infty} \sum_{n=-\infty}^{+\infty}$$

Using the identity:

$$\sum_{m,n} e^{-i(\overline{k}-\overline{k}_t)\cdot \overline{r}_{mn}} = \frac{4\pi^2}{A} \sum_{m,n} \delta(\overline{k} - \overline{k}_{t_{mn}}) \tag{5.8}$$

and the spectral representation:

$$g(\overline{r}, \overline{r}') = \frac{i}{(2\pi)^2} \int_{-\infty}^{+\infty} \int_{-\infty}^{+\infty} \frac{1}{2k_z} e^{i\overline{k}_t \cdot (\overline{r}_t - \overline{r}'_t) + ik_z |z-z'|} dk_x dk_y \tag{5.9}$$

with $\overline{r}_t = x\hat{x} + y\hat{y}$, equation (5.7) gives the spectral representation of the two-dimensional periodic Green's function:

$$g_p(\overline{r}, \overline{r}') = \sum_{m,n} \frac{1}{i2Ak_{z_{mn}}} e^{i\overline{k}_{t_{mn}} \cdot (\overline{r} - \overline{r}') + ik_{z_{mn}} |z-z'|} \tag{5.10}$$

where for simplicity it is assumed that the reference source is at the origin, where A is the area of the unit cell and:

$$k_{z_{mn}} = \begin{cases} \sqrt{k^2 - \left|\overline{k}_{t_{mn}}\right|^2}, & k > \left|\overline{k}_{t_{mn}}\right| \\ \\ i\sqrt{\left|\overline{k}_{t_{mn}}\right|^2 - k^2}, & k < \left|\overline{k}_{t_{mn}}\right| \end{cases} \tag{5.11}$$

$$\overline{k}_{t_{mn}} = (m + m_0)\overline{k}_1 + (n + n_0)\overline{k}_2 \tag{5.12}$$

90

where:

$$\bar{k}_1 = \left(\frac{2\pi}{d_x}\right)\hat{x} \tag{5.13}$$

$$\bar{k}_2 = \left(\frac{2\pi}{d_y}\right)\hat{y} \tag{5.14}$$

$$m_0 = \frac{k}{|\bar{k}_1|}\sin\theta_0\cos\phi_0 \tag{5.15}$$

$$n_0 = \frac{k}{|\bar{k}_2|}\sin\theta_0\sin\phi_0 \tag{5.16}$$

$\bar{k}_1, \bar{k}_2$ are the reciprocal lattice phase vectors, d_x, d_y are the periodicities in the x and y directions, respectively, m_0, n_0 are the interelement phase shift constants, θ_0, ϕ_0 define the direction of the main beam and k is the free space wavenumber. The spatial representation of the periodic Green's function is [19]:

$$g_p(\bar{r},\bar{r}') = \frac{1}{4\pi}\sum_{m,n}e^{i2\pi(mm_0+nn_0)}\frac{e^{ikR_{mn}}}{R_{mn}} \tag{5.17}$$

where:

$$R_{mn} = |\bar{r} - \bar{r}'_{mn}| \tag{5.18}$$

Note that in the case of normal incidence, that is $\theta_0 = 0$ the interelement phase constants m_0 and n_0 are zero.

5.3 Two-Dimensional Arrays of Helices

In our analysis the helix axis is along the z-direction and the helices are aligned and periodically spaced on the $x - z$ plane with periodicities d_x and d_z along the x and z directions, respectively. Therefore the expressions (5.3) and (5.4) are:

$$\bar{r}_{mn} = md_x\hat{x} + nd_y\hat{y} \tag{5.19}$$

$$\bar{r}'_{mn} = \bar{r}' + \bar{r}_{mn} \tag{5.20}$$

91

where $\bar{r}'$ is the source point on the center helix as defined in the analysis of Section 4.2.

Considering the case of normal incidence along the y direction $\overline{E}^i = \overline{E}_0 e^{iky}$, the equations (5.10) and (5.17) for the periodic Green's function become:

$$g_p(\bar{r}, \bar{r}') = \sum_{m,n} \frac{1}{i2Ak_{y_{mn}}} e^{ik_{y_{mn}}|y-y'| + i\bar{k}_{t_{mn}} \cdot (\bar{r}-\bar{r}')} \tag{5.21}$$

where:

$$k_{y_{mn}} = \begin{cases} \sqrt{k^2 - \left|\bar{k}_{t_{mn}}\right|^2}, & k > \left|\bar{k}_{t_{mn}}\right| \\ \\ i\sqrt{\left|\bar{k}_{t_{mn}}\right|^2 - k^2}, & k < \left|\bar{k}_{t_{mn}}\right| \end{cases} \tag{5.22}$$

and

$$\bar{k}_{t_{mn}} = m\left(\frac{2\pi}{d_x}\right)\hat{x} + n\left(\frac{2\pi}{d_z}\right)\hat{z} \tag{5.23}$$

In our approach we use the spatial representation of the periodic Green's function in order to avoid the singularity $\hat{y}\hat{y}\delta(y - y')$ that appears in the spectral representation of the dyadic periodic Green's function. We also consider the case of normal incidence along the y direction, therefore the interelement phase shift constants are zero:

$$\overline{\overline{G}}_p(\bar{r}, \bar{r}') = \left(\overline{\overline{I}} + \frac{1}{k^2}\nabla\nabla\right) g_p(\bar{r}, \bar{r}') = \frac{1}{4\pi k^2} \sum_{m,n} \left(k^2\overline{\overline{I}} + \nabla\nabla\right)\frac{e^{ikR_{mn}}}{R_{mn}} \tag{5.24}$$

where now:

$$R_{mn} = |\bar{r} - \bar{r}' - (md_x\hat{x} + nd_z\hat{z})| \tag{5.25}$$

Because:

$$\nabla\nabla\frac{e^{ikR_{mn}}}{R_{mn}} = \frac{(ikR_{mn} - 1)}{R_{mn}^2}\overline{\overline{I}} + \frac{3(1 - ikR_{mn}) - (kR_{mn})^2}{R_{mn}^2}\hat{R}_{mn}\hat{R}_{mn} \tag{5.26}$$

The final form of (5.24) is :

$$\begin{aligned} \overline{\overline{G}}_p(\bar{r}, \bar{r}') &= \frac{1}{4\pi k^2} \sum_{m,n} \left[\frac{(kR_{mn})^2 - (1 - ikR_{mn})}{R_{mn}^2}\overline{\overline{I}} \right. \\ &\left. + \frac{3(1 - ikR_{mn}) - (kR_{mn})^2}{R_{mn}^2}\hat{R}_{mn}\hat{R}_{mn} \right] \frac{e^{ikR_{mn}}}{R_{mn}} \end{aligned} \tag{5.27}$$

Through the use of the periodic Green's function, the scattering problem is reduced to that of the center helix. The analysis is similar to that of Chapter 4. The scattered field is:

$$\overline{E}^s(\overline{r}) = i\omega\mu \int_0^{\Phi} d\phi' \overline{\overline{G}}_p(\overline{r}, \overline{r}') I(\phi') t\hat{t}'(\phi') \tag{5.28}$$

or, using (5.27):

$$\begin{aligned}
\overline{E}^s &= \frac{i\eta}{4\pi k} \sum_{m,n} \int_0^{\Phi} d\phi' \left[\frac{(kR_{mn})^2 - (1 - ikR_{mn})}{R_{mn}^2} \overline{\overline{I}} \right. \\
&\quad + \left. \frac{3(1 - ikR_{mn}) - (kR_{mn})^2}{R_{mn}^2} \hat{R}_{mn}\hat{R}_{mn} \right] \frac{e^{ikR_{mn}}}{R_{mn}} I(\phi') t\hat{t}'(\phi') \tag{5.29}
\end{aligned}$$

We apply now the boundary condition for the electric field on the wire surface assuming perfectly conducting helices. The position and tangential vectors on the axis and the surface of the center helix are defined as in Chapter 3.

$$\begin{aligned}
-s\hat{t}(\phi)\overline{E}^i &= \frac{i\eta}{4\pi k} \sum_{m,n} \int_0^{\Phi} d\phi' I(\phi') \left[\frac{(kR_{mn})^2 - (1 - ikR_{mn})}{R_{mn}^2} s\hat{t}(\phi) \cdot \hat{t}'(\phi') \right. \\
&\quad + \left. \frac{3(1 - ikR_{mn}) - (kR_{mn})^2}{R_{mn}^2} (s\hat{t}(\phi) \cdot \hat{R}_{mn})(t \cdot \hat{t}'(\phi')\hat{R}_{mn}) \right] \frac{e^{ikR_{mn}}}{R_{mn}} \tag{5.30}
\end{aligned}$$

where $\overline{E}^i = \overline{E}_0 e^{iky} = \overline{E}_0 e^{ik\rho \sin\phi}$ and:

$$s\hat{t}(\phi) \cdot \hat{t}'(\phi') = b(a + b)\cos(\phi - \phi') + \left(\frac{P}{2\pi}\right)^2 \tag{5.31}$$

$$s\hat{t}(\phi) \cdot \hat{R}_{mn} = \frac{1}{R_{mn}} \left\{ b(a + b)\sin(\phi - \phi') + \frac{P}{2\pi}\left[\frac{p}{2\pi}(\phi - \phi') - nd_z\right] + m(a + b)d_x \sin\phi \right\} \tag{5.32}$$

$$t\hat{t}'(\phi') \cdot \hat{R}_{mn} = \frac{1}{R_{mn}} \left\{ b(a + b)\sin(\phi - \phi') + \frac{P}{2\pi}\left[\frac{P}{2\pi}(\phi - \phi') - nd_z\right] + mbd_x \sin\phi' \right\} \tag{5.33}$$

The integral equation is again discretized and Galerkin's method is applied on the center helix, using triangular basis and testing functions $f_N(\phi)$. The matrix equation for the current on the helix is:

$$V_M = \sum_N Z_{MN} I_N \tag{5.34}$$

93

where:

$$V_M = - \int_{D_M} d\phi s\hat{t}(\phi) \cdot \overline{E}_0 e^{ik(a+b)\sin\phi} f_M(\phi) d\phi \tag{5.35}$$

$$
\begin{aligned}
Z_{MN} = \ & \frac{i\eta}{4\pi k} \sum_{m,n} \int_{D_M} d\phi f_M(\phi) \int_{D_N} d\phi' f_N(\phi') \left[\frac{(kR'_{mn})^2 - (1 - ikR_{mn})}{R^2_{mn}} s\hat{t}(\phi) \cdot \hat{t}'(\phi') \right. \\
& + \left. \frac{3(1 - ikR_{mn}) - (kR_{mn})^2}{R^2_{mn}} (s\hat{t}(\phi) \cdot \hat{R}_{mn})(t\hat{t}'(\phi') \cdot \hat{R}_{mn}) \right] \frac{e^{ikR_{mn}}}{R_{mn}} \tag{5.36}
\end{aligned}
$$

In this case, as it can be seen in (5.32) and (5.33) the integrand does not depend only on the difference $v = \phi - \phi'$ so the integral cannot be simplified to a single one. When the induced currents are obtained the scatterd field can be calculated from (5.29). The expression for the far field can be obtained by making the approximations:

$$\sqrt{|\bar{r} - \bar{r}_{mn}|^2 - 2(\bar{r} - \bar{r}_{mn}) \cdot \bar{r}' + |\bar{r}'|^2} = R_{mn} \sqrt{1 - 2\frac{\hat{R}_{mn}}{R_{mn}} \cdot \bar{r}' + \frac{|\bar{r}'|^2}{R^2_{mn}}} \tag{5.37}$$

where now $R_{mn} = |\bar{r} - \bar{r}_{mn}|$, so finally:

$$\sqrt{|\bar{r} - \bar{r}_{mn}|^2 - 2(\bar{r} - \bar{r}_{mn}) \cdot \bar{r}' + |\bar{r}'|^2} \simeq R_{mn} - \hat{R}_{mn} \cdot \bar{r}' \tag{5.38}$$

for the exponentials, and:

$$\sqrt{|\bar{r} - \bar{r}_{mn}|^2 - 2(\bar{r} - \bar{r}_{mn}) \cdot \bar{r}' + |\bar{r}'|^2} \simeq R_{mn} \tag{5.39}$$

for all others.

If we drop the terms of order $\frac{1}{R^l_{mn}}$, $l > 1$ then the far field approximation of (5.29) gives:

$$\overline{E}^s = \frac{i\eta k}{4\pi} \sum_{m,n} \frac{e^{ikR_{mn}}}{R_{mn}} \left(\overline{\overline{I}} - \hat{R}_{mn} \hat{R}_{mn} \right) \int_0^{\Phi} d\phi' I(\phi') t\hat{t}'(\phi') e^{-ik\hat{R}_{mn} \cdot \bar{r}'} \tag{5.40}$$

We calculate the scatterd field for $\phi = \pm\frac{\pi}{2}$ and $z = 0$ so:

$$\hat{R}_{mn} = \frac{\overline{R}_{mn}}{R_{mn}} = \frac{-md_x\hat{x} \pm \rho\hat{y} - nd_z\hat{z}}{\sqrt{\rho^2 + (md_x)^2 + (nd_z)^2}} \qquad (5.41)$$

$$\hat{R}_{mn} \cdot \overline{r}' = \frac{-md_xb\cos\phi' \pm \rho b\sin\phi' - \frac{p}{2\pi}\phi' nd_z}{\sqrt{\rho^2 + (md_x)^2 + (nd_z)^2}} \qquad (5.42)$$

We define the radiation vector as:

$$\overline{N}_{mn} = \int_0^{\Phi} d\phi' I(\phi') t\hat{t}'(\phi') e^{-ik\hat{R}_{mn}\cdot\overline{r}'} \qquad (5.43)$$

with components:

$$N_{mn_x} = -\int_0^{\Phi} d\phi' I(\phi') b\sin\phi' e^{-ik\hat{R}_{mn}\cdot\overline{r}'} \qquad (5.44)$$

$$N_{mn_y} = \int_0^{\Phi} d\phi' I(\phi') b\cos\phi' e^{-ik\hat{R}_{mn}\cdot\overline{r}'} \qquad (5.45)$$

$$N_{mn_z} = \int_0^{\Phi} d\phi' I(\phi') \frac{p}{2\pi} e^{-ik\hat{R}_{mn}\cdot\overline{r}'} \qquad (5.46)$$

and

$$\hat{R}_{mn} \cdot \overline{N}_{mn} = \frac{-md_x N_{mn_x} \pm \rho N_{mn_y} - nd_z N_{mn_z}}{\sqrt{\rho^2 + (md_x)^2 + (nd_z)^2}} \qquad (5.47)$$

Due to symmetry along x and z directions, we assume that the contributions to the scattered field from the y components of the currents cancel, thus only the x and z components of the scattered electric field remain. The components of the scattered field that we calculate are:

$$E_x^s = \frac{i\eta k}{4\pi} \sum_{m,n} \left[N_{mn_x} + \frac{md_x}{R_{mn}^2}(\overline{R}_{mn} \cdot \overline{N}_{mn}) \right] \frac{e^{ikR_{mn}}}{R_{mn}} \qquad (5.48)$$

$$E_z^s = \frac{i\eta k}{4\pi} \sum_{m,n} \left[N_{mn_z} - \frac{nd_z}{R_{mn}^2}(\overline{R}_{mn} \cdot \overline{N}_{mn}) \right] \frac{e^{ikR_{mn}}}{R_{mn}} \qquad (5.49)$$

An extension of this analysis is next applied to the case of a superposition of periodic layers of helices.

5.4 Three-Dimensional Arrays of Helices

A three dimensional periodic structure will be considered along the y-direction as a superposition of a finite number of periodic layers. The analysis of the electromagnetic scattering is an extension to that of a single layer. Our objective is to find the transmitted and reflected fields when this three-dimensional periodic structure is illuminated by an incident plane wave.

Consider L such layers at distance d apart. The axis of the helices of the l–th layer are in the plane $y = ld$ with $l = 0...L - 1$. In this case the scattered field is a superposition of the contributions to the scattering due to the currents on each layer.

$$\overline{E}^s = \frac{i\eta}{4\pi k} \sum_{m,n} \int_0^{\Phi} \left(k^2 \overline{\overline{I}} + \nabla\nabla\right) \sum_{l=0}^{L-1} \frac{e^{ikR_{mn_l}}}{R_{mn_l}} I_l(\phi') t\hat{t}'(\phi') \qquad (5.50)$$

where l corresponds to the helix of thr lth layer and:

$$R_{mn_l} = |\overline{r} - \overline{r}'_{mnl}| \qquad (5.51)$$

where now the source point is on the l–th layer.

$$\overline{r}'_{mnl} = \overline{r}' + \overline{r}_{mn} + ld\hat{y} \qquad (5.52)$$

and

$$\overline{r}_{mn} = md_x\hat{x} + nd_z\hat{z} \qquad (5.53)$$

The boundary condition for the electric field on the wire surface of the helix on each layer j is applied resulting in a matrix integral equation:

$$- s\hat{t}(\phi) \cdot \overline{E}_0 e^{ik[(a+b)\sin\phi + jd]} = \frac{i\eta}{4\pi k} \sum_{l=0}^{L-1} \sum_{m,n} \int_0^{\Phi} d\phi' s\hat{t}(\phi) \left(k^2 \overline{\overline{I}} + \nabla\nabla\right) \frac{e^{ikR_{mn_{(l-j)}}}}{R_{mn_{(l-j)}}} t\hat{t}'(\phi') \qquad (5.54)$$

The current I_l for each layer l is expanded as:

$$I_l(\phi) = \sum_{N_l} I_{N_l} f_{N_l}(\phi') \qquad (5.55)$$

Galerkin's method is applied and the resulting matrix equation for the unknown vectors of the expasion coefficients I_{N_l} is:.

$$
\begin{bmatrix} \overline{V}_0 \\ \cdot \\ \cdot \\ \overline{V}_j \\ \cdot \\ \cdot \\ \overline{V}_{L-1} \end{bmatrix} = \begin{bmatrix} \overline{\overline{Z}}_{00} & \cdots & \overline{\overline{Z}}_{0l} & \cdots & \overline{\overline{Z}}_{LL} \\ \cdot & & \cdot & & \cdot \\ \cdot & & \cdot & & \cdot \\ \overline{\overline{Z}}_{j0} & \cdots & \overline{\overline{Z}}_{jl} & \cdots & \overline{\overline{Z}}_{jL} \\ \cdot & & \cdot & & \cdot \\ \cdot & & \cdot & & \cdot \\ \overline{\overline{Z}}_{L0} & \cdots & \overline{\overline{Z}}_{Ll} & \cdots & \overline{\overline{Z}}_{LL} \end{bmatrix} \begin{bmatrix} \overline{I}_0 \\ \cdot \\ \cdot \\ \overline{I}_l \\ \cdot \\ \cdot \\ \overline{I}_L \end{bmatrix} \tag{5.56}
$$

where $\overline{V}_j$ is the vector of excitations for the $j-$th layer:

$$
\overline{V}_j = \begin{bmatrix} V_{1_l} \\ \cdot \\ \cdot \\ V_{M_l} \\ \cdot \\ \cdot \\ V_{Nmax_l} \end{bmatrix} \tag{5.57}
$$

with:

$$
V_{M_l} = \int_{D_{M_j}} d\phi \left[-s\hat{t}(\phi) \cdot \overline{E}_0 e^{ik[(a+b)\sin\phi + jd]} \right] f_M(\phi) \tag{5.58}
$$

and $\overline{\overline{Z}}_{jl}$ is the impedance matrix that describes the coupling between the helix of the $j-$th layer where the testing is done and the $l - th$ layer where the source is.

$$
\overline{\overline{Z}}_{jl} = \begin{bmatrix} Z_{11_{jl}} & \cdots & Z_{1N_{jl}} & \cdots & Z_{1Nmax_{jl}} \\ & \cdot & & \cdot & & \cdot \\ & \cdot & & \cdot & & \cdot \\ Z_{M1_{jl}} & \cdots & Z_{MN_{jl}} & \cdots & Z_{MNmax_{jl}} \\ & \cdot & & \cdot & & \cdot \\ & \cdot & & \cdot & & \cdot \\ Z_{Nmax1_{jl}} & \cdots & Z_{NmaxN_{jl}} & \cdots & Z_{NmaxNmax_{jl}} \end{bmatrix} \tag{5.59}
$$

with

$$
Z_{MN_{jl}} = \frac{i\eta}{4\pi k} \sum_{l=0}^{L} \sum_{m,n} \int_{D_{M_j}} d\phi f_{M_j}(\phi) \int_{D_{N_l}} d\phi' f_{N_l}(\phi') s\hat{t}(\phi) \left(k^2 \overline{\overline{I}} + \nabla\nabla \right) \frac{e^{ikR_{mn_{(l-j)}}}}{R_{mn_{(l-j)}}} t\hat{t}'(\phi') \tag{5.60}
$$

while $\overline{R}_{mn_{(l-j)}}$ is the vector from the testing point on the center helix of the $j-$th layer to the source point on the (m,n)-helix of the $l-$ layer:

$$
R_{mn_{(l-j)}} = \left\{ [(a+b)\cos\phi - (b\cos\phi' + md_x)]^2 + [(a+b)\sin\phi - jd - (b\sin\phi' + ld)]^2 + [P/2\pi(\phi - \phi') - nd_z]^2 \right\}^{1/2} \tag{5.61}
$$

Solving for the currents on the helices of each layer the scattered fields can be calculated as in the previous section for the given excitation.

In this configuration the helices are aligned so that the periodic structure behaves as anisotropic medium [9]. However, we can study its behaviour for specific polarization of the incident wave and calculate the copolarized and crosspolarized scattered fields. Hence we can derive conclusions about the chirality that this structure exhibits.

5.5 Summary

In this chapter the first step has been made for an alternate approach to studying the electromagnetic responce of helix loaded composites. The simplest case of periodic helix structures has been considered and our analysis was focussed on finding the currents induced on the helices, which is the first step for calculating the reflection and

transmission coefficients. Then, we can calculate the copolarized and the crosspolarized components of the transmitted wave, thus determining its polarization ellipse. These calculations can be related to the chirality of this superposition of periodic layers, based on the discussion of Section 2.4. The chirality could be found in terms of the distance d between them. It would be desirable to have results for chirality independent of the number of layers so that the superposition of a finite number of them would simulate a chiral slab.

The formulation for this approach has been derived with the use of the spatial representation of the two dimensional periodic Green's function. The extension of the method of moments to the case of periodic arrays and superposition of arrays has been used as an accurate solution of the scattering problem and a numerical code has been implemented and tested for the case of a single layer. The induced currents that are obtained for sparse stuctures agree with those for a single helix while in the case of dense arrays different results are expected due to the coupling between adjacent helices. This case is still under investigation as well as the three-dimensional structure.

Therefore, there are issues to be addressed in a further work on this approach. Because the evaluation of infinite double sums is involved in the calculations, large amounts of CPU time are required to examine a single case. For a further investigation, an acceleration technique may be needed for the evaluation of the infinite double sum in the periodic Green's function.

Bibliography

[1] A. J. Bahr and K. R. Clausing. An approximate model for artificial chiral material. *IEEE Transactions on Antennas and Propagation*, 42(12):1592–1598, December 1994.

[2] V. V. Varadan, A. Lakhtakia and V. K. Varadan. A parametric study of a planar achiral-chiral interface. *IEEE Transactions on Electromagnetic Compatibility*, 28(2):90–95, May 1986.

[3] A. Sezginer and J. A. Kong. Physical optics approach for scattering by thin helical wires. *Radio Science*, 18(5):639–649, September-October 1983.

[4] C. F. Bohren. Light scattering by an optically active sphere. *Chemical Physics Letters*, 29(3):458–462, December 1974.

[5] D. K. Ghodgaonkar, V. V. Varadan and V. K. Varadan. Free-space measurements of complex permittivity and complex permeability of magnetic materials at microwave frequencies. *IEEE Transactions on Instrumentation and Measurement*, 39:387–394, 1990.

[6] D. L. Jaggard, A. R. Michelson and C. H. Papas. On electromagnetic waves in chiral media. *Applied Physics*, 18:211–216, 1979.

[7] I. V. Lindell and A. H. Sihvola. Chiral Maxwell-Garnett mixing formula. *Electronics Letters*, 26(2):118–119, January 1990.

[8] I. V. Lindell and A. H. Sihvola. Quasi-static analysis of scattering from a chiral sphere. *Journal of Electromagnetic Waves and Applications*, 4(12):1223–1231, 1990.

[9] S. A. Tretyakov, I. V. Lindell, A. H. Sihvola and A. J. Viitanen. *Electomagnetic Waves in Chiral and Bi-Isotropic Media*. Artech House, 1994.

[10] E. H. Newman, J. L. Blanchard and M. E. Peters. Integral equation analysis of artificial media. *IEEE Transactions on Antennas and Propagation*, 42(5):727–731, May 1994.

[11] Jin Au Kong. *Electromagnetic Wave Theory*. John Wiley & Sons Inc., 1990.

[12] K. F. Lindman. *Ann. Phys.*, 63:621, 1920.

[13] K. F. Lindman. *Ann. Phys.*, 69:270, 1922.

[14] L. Pasteur. *Ann. Chim. et Phys.*, 24:442–459, 1848.

[15] R. D. Hollinger, V. V. Varadan, D. K. Ghodhaonkar, and V. K. Varadan. Experimental characterization of isotropic chiral composites in circular waveguides. *Radio Science*, 27(2):161–168, March-April 1992.

[16] R. E. Raab and J. H. Cloete. An eigenvalue theory of circular birefringence and dichroism in a non-magnetic chiral medium. *Journal of Electromagnetic Waves and Applications*, 8(8):1073–1089, 1994.

[17] H. S. Langdon, R. Luebbers, F. Hunsberger, C. F. Bohren and S. Yoshikawa. Calculation an measurement of the effective chirality parameter of a composite chiral material over a wide frequency band. *IEEE Transactions on Antennas and Propagation*, 43(2):123–129, February 1995.

[18] V. V. Varadan, R. Ro and V. K. Varadan. Electromagnetic activity and absorption in microwave chiral composites. *IEE Proceedings-H*, 139(5):441–448, October 1992.

[19] W. F. Richards, S. Singh, J. R. Zinecker, and D. R. Wilton. Accelerating the convergence of series representing the free space periodic green's function. *IEEE Transactions on Antennas and Propagation*, 38(12):1958–1962, December 1990.

[20] S. Singh and R. Singh. On the use of levin's t-transform in accelerating the summation of series representing the free-space periodic green's functions. *IEEE Transactions on Microwave Theory and Techniques*, 41(5):884–886, May 1993.

[21] T. Guire, V. V. Varadan and V. K. Varadan. Influence of chirality on the reflection of em waves by planar dielectric slabs. *IEEE Transactions on Electromagnetic Compatibility*, 32:300–304, 1990.

[22] V. V. Varadan, V. K. Varadan and A. Lakhtakia. On the possibility of designing anti-reflection coatings using chiral composites. *Journal of Wave-Material Interaction*, 2(1):71–81, January 1987.

[23] A. Lakhtakia, V. V. Varadan and V. K. Varadan. Equivalent dipole moments of helical arrangements of small, isotropic, point-polarizable scatters: Application to chiral polymer design. *Journal of Applied Physics*, 63(2):90–95, January 1988.

[24] A. Lakhtakia, V. V. Varadan and V. K. Varadan. Microscopic circular polarizabilities (rotabilities) and the macroscopic properties of chiral media. *Radio Science*, 26(2):511–516, March-April 1991.

[25] V. V. Varadan, R. Ro and V. K. Varadan. Measurement of the electromagnetic properties of chiral composite materials in the 8-40 ghz range. *Radio Science*, 29(1):9–22, January-February 1994.

[26] Y. Ma, V. V. Varadan and V. K. Varadan. Effects of chiral microstructure on em propagation in discrete random media. *Radio Science*, 24(6):785–792, November-December 1989.

[27] Johnson J. H. Wang. *Generalized Moment Methods in Electromagnetics, Formulation and Computer Solution of Integral Equations*. John Wiley & Sons Inc., 1991.

[28] K. W. Whites. Full-wave computation of constitutive parameters for lossless composite chiral materials. *IEEE Transactions on Antennas and Propagation*, 43(4):376–384, April 1995.